The present study was aimed at resolving the question - could such a dynamic movement as external ear also be explained by differential growth? MR imaging data of human embryos from the Kyoto Collection of Human Embryos [13]; http://bird.cac.med.kyoto-u.ac.jp] was used for tracing the 3D absolute position of the anatomical landmarks. The MR data had the advantage of comparing facial structures between different stages with identical magnification. Data revealed that positional changes of external and internal ears that occur during morphogenesis could be explained by differential growth.

Materials and methods

Human embryo specimens

Around 44,000 human embryos (constituting the Kyoto Collection) were historical specimens collected and stored at the Congenital Anomaly Research Center of Kyoto University [14-16]. In most cases, pregnancy was terminated during the first trimester for socioeconomic reasons under the Maternity Protection Law of Japan. Some of the specimens (~20%) were undamaged, well-preserved embryos. When the aborted materials were brought to the laboratory, the embryos were measured, examined, and staged using the criteria of O'Rahilly and Müller [10]. Approximately 1,200 well-preserved human embryos diagnosed as externally normal at CS 13 to CS 23 were selected for MR microscopic imaging. The conditions used to acquire the MR images of the embryos are described elsewhere [17,18].

MR image processing and selection of datasets

3D MR image datasets for each embryo were initially obtained from 256 × 256 × 512 voxels. Each dataset was first converted into a two-dimensional (2D) stack and saved as an audio video interleave (.avi) file format using software ImageJ™ (version 1.42q, National Institutes of Health, Bethesda, MD). Sequential 2D images were resectioned digitally and 3D images were reconstructed using the software OsiriX™ (version 3.7.1, Pixmeo SARL, Geneva, Switzerland). Both 2D and 3D images were carefully observed and selected according to the following conditions: 1) no obvious damage or significant anomaly present in the external appearance; 2) body axes maintained in the original form, i.e. not deformed artificially during fixation and preservation; 3) sufficiently high quality of reconstructed 2D images to properly extract the organs and tissues. For the present study, 171 samples between CS 17 and 23 were selected from all 1,200 MR image datasets based on the criteria described above. The number of cases for each CS was distributed between 18 and 30.

Anatomical landmarks

The 3D coordinate was initially given for 13 selected landmarks by examining the position of the voxel on 2D sequential and 3D images using OsiriX (Figure 1). The selected 13 landmarks were as follows: bilateral auricular hillock on the first cranial arch which becomes tragus later (Ex1), bilateral auricular hillock on the second cranial arch which becomes antitragus later (Ex6) and vestibule (Int) as representative external and internal ear landmarks; stomodeum which becomes a part of mouth (Mo), bilateral nasal pits (Np), bilateral lens vesicles which become a part of eyes (Ey) as external anatomical landmarks, and infundibulum of diencephalons (later pituitary gland) (Pg) and cranial region of the first cervical vertebra (C1) as internal anatomical landmarks.

Evaluation of the position of anatomical landmarks

Two kinds of methods were used to evaluate and analyze the position of the anatomical landmarks in the present study (Figure 2A). Method-1 was used for evaluating the absolute position while Method-2 was for the relative position of each landmark.

Method-1 (Measurement of the absolute position) The 3D absolute position of the anatomical landmarks from MR image data was used to compare the position of each anatomical landmark between the different stages with identical magnification. The line connecting C1 and Pg was defined as reference axis (Z-axis) of 3D orthogonal coordinate for this purpose. Both C1 and Pg are less mobile internal structures close to notocord and detectable during the development [1,19]. Distances between bilateral Ex1s, and collateral Ex1 and Int were calculated and defined as L_{EE} and L_{EI} respectively (Figure 2B). The middle point of the collateral Ex1 and Ex6 were defined as Exm.

Method-2 (Measurement of the relative position) The relative position of the external ears with other landmarks during craniofacial morphogenesis was observed from the frontal position of the face at each stage. For this purpose, the line connecting the middle point of the bilateral Eys and Pg was defined as reference axis (X-axis). The vertical line to the X-axis which contained Mo was defined as Z-axis of 3D orthogonal coordinate. The XY plane defined by this method was almost parallel to the structures at the base of the skull, which divide the area between the neurocranium and viscerocranium [1]. Further, the distance between the middle point of bilateral Eys and Mo was kept constant at one so as to adjust the expansive growth of the face (Figure 2A).

This study was approved by The Committee of Medical Ethics of Kyoto University Graduate School of Medicine, Kyoto, Japan (E986).

Results

Absolute position of internal and external ear and anatomical landmarks

The 3D absolute position of the anatomical landmarks was shown using Method-1. All landmarks moved away

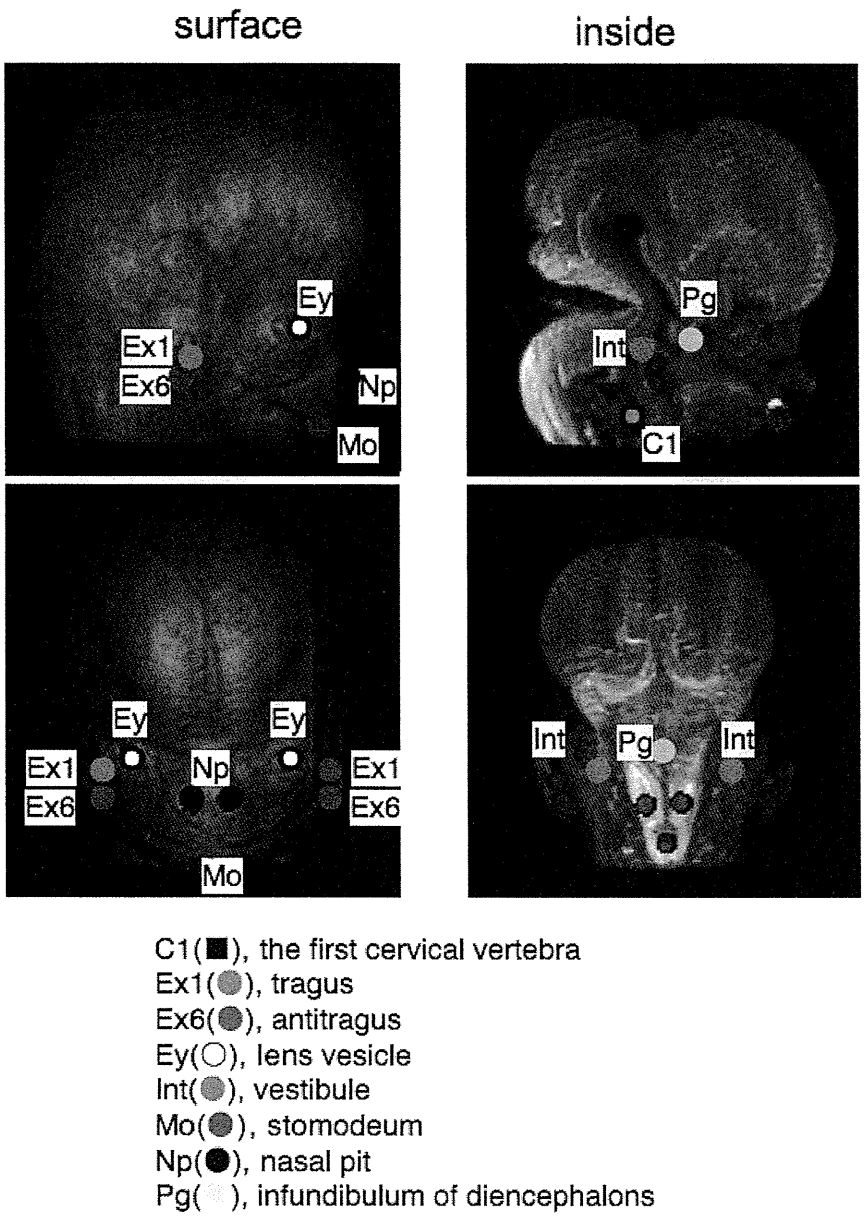

Figure 1 The 13 landmarks selected for present study. Landmarks were expressed on volume rendering 3D images of the head region for surface and maximum intensity projection for inside constructed with software OsiriX.

from the origin (C1) by frontal view (Figure 3A). The line connecting Pg, Ey and Np became longer, which might indicate swelling of the face. Ex1, Ex6 and Int also moved away from the origin (C1) like other landmarks, except that the movement of Int between CS 17 and CS 20 was slow.

By right lateral view, the lines connecting Pg, Ey, Np and Mo, resembling the side view of the swelling face, also became larger as development proceeded (Figure 3B). The movement of Ex1, Ex6 and Int was different from that of the other landmarks. They rotated clockwise for Ex1 and anti-clockwise for Ex6 and Int around CS 17 and CS 21; after that, they moved dorso-cranially.

The position of each landmark in the cranial direction between CS 17 and CS 23 was demonstrated (Figure 3C). All landmarks changed positions smoothly and

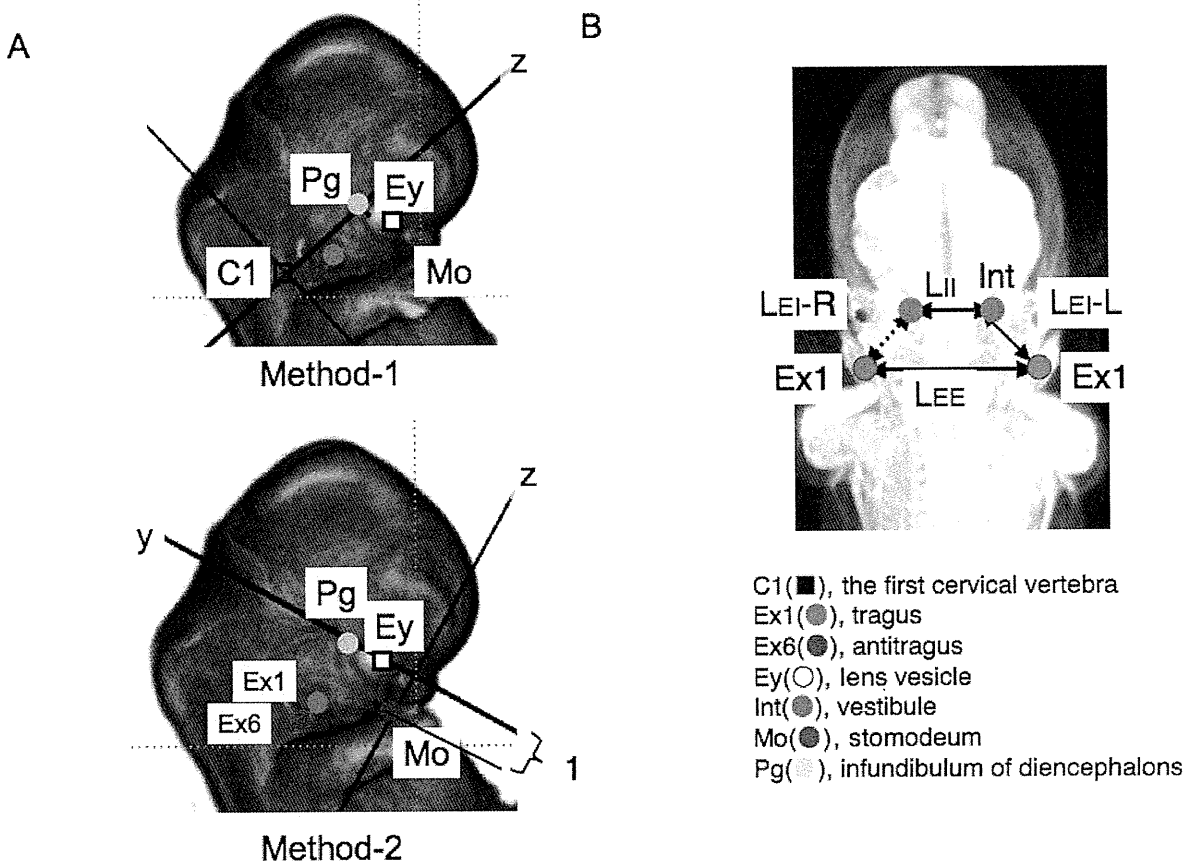

Figure 2 Lateral view showing reference axes, anatomical landmarks and morphometry in present study (A) Reference axes used in Method-1 and Method-2. Reference axes and landmarks were expressed on volume rendering 3D images of the head region constructed with software OsiriX. (B) Anatomical landmarks and morphometry measured in present study. Landmarks were expressed on maximum intensity projection 3D images of the head region constructed with software OsiriX for inside viewing. Distances between bilateral Ex1s, bilateral Ints and collateral Ex1 and Int were defined as L_{EE}, L_{EI}, and L_{EI}, respectively.

gradually during development. As for Int, Ex1, and Ex6, the movement of the position along the cranial/caudal direction was very limited.

Distance and 3D relationship between internal and external ear

L_{EE} and L_{II} increased as CS proceeded (Figure 4). L_{EE} at CS 17 was 2.43+/-0.20 mm (mean +/-SD), and reached 7.38 +/-0.72 mm at CS23. L_{II} at CS 17 was 2.52+/-0.18 mm, and reached 4.63+/-0.41 mm at CS 23. L_{EE} may correspond to the lateral growth of the face, whereas L_{II} corresponds to the lateral thickness of the neural tube. Interestingly, both L_{EI}-L and L_{EI}-R were kept approximately constant, with distribution between 1.42 and 2.01 mm.

Three-dimensionally, the external ear (Exm) located vent-caudal parts of the internal ear in CS 17, and then moved mainly laterally (Figure 5). Exm rotated approximately 49 degrees during CS 17 and CS 23 when Int was the origin (data not shown).

Relative movement of external and internal ear

The relative movement of anatomical landmarks including Ex1, Ex6, and Int was demonstrated using Method-2 (Figure 6). Most landmarks gathered toward the origin as CS proceeded. The relative movement was noticeably larger in Ex1, Ex6, and Int than in Eys, Np, and Pg. Ex1 and Ex6 moved from the caudal lateral ventral region toward the origin. They moved with high speed between CS 17 and 20, and then located and almost stayed between Eys and Mo after CS 21 (Figure 6C). Int migrated from the caudal dorsal lateral region and almost stayed there after CS 21 as well.

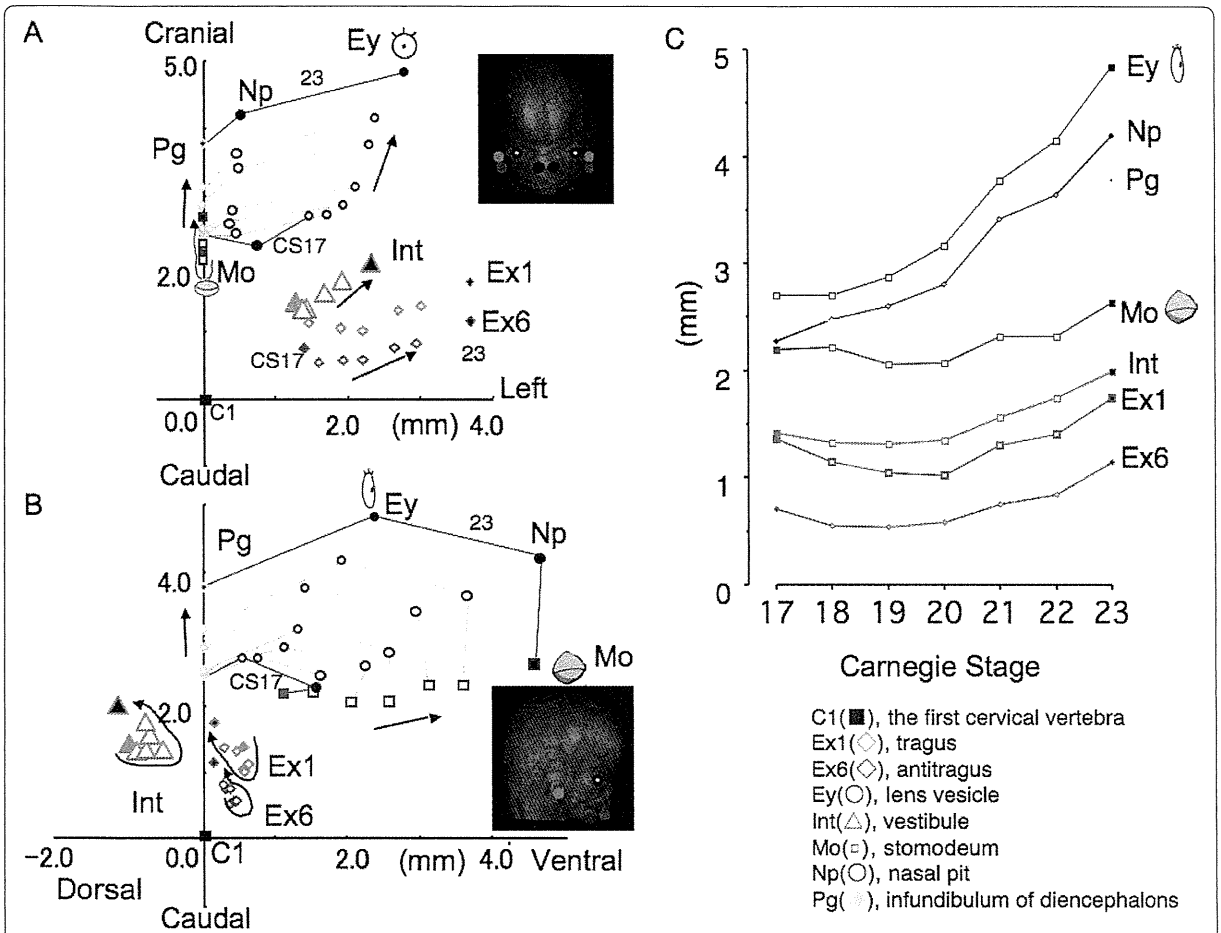

Figure 3 Movement of external and internal ear and anatomical landmarks during development in the orthogonal coordinate defined in Method-1. Frontal view (A) and lateral view (B). The line which connects the pituitary gland and the first cervical vertebra was reference axis (Z-axis) (See also Figure 2). (C). Movement of anatomical landmarks along the reference (Z)-axis.

Discussion

In a recent study, Gasser [12] proposed that some events of mammalian embryogenesis can result from differential growth. Gasser pointed out that dramatic changes occur in size and shape of the embryo and its internal structures but these changes were not considered in past studies that described migratory movements. The present study was performed to reveal whether the movement of human external ears could also be explained as differential growth.

As a principle of physics, all movements occur in relation to a reference point. Thus, it is important to select appropriate references. Gasser [12] claimed that the ideal reference point would be one in the center of the mass, i.e. a centroid. Even though no such consistently occurring point exists in developing embryos, any point that is more centrally located would move less in relation to surrounding structures and therefore would be more suitable. Two methods were used to evaluate the position of the anatomical landmarks in the present study. Method-1 was planned according to Gasser's opinion. The authors selected both C1 and Pg as an ideal reference axis. These were the most central of the embryonic structures located along the notochord. The notochord is an important structure for vertebrate animals, determining the cranial/caudal axis and dividing left and right. It runs along the neural tube and the anterior tip of the notochord reaches an area where the Pg starts to develop [1,19]. C1 body segment is used as one of the reference points in Gasser's study [12]. Another reason for selecting these points was that both were clearly detectable in all stages analyzed.

Movement of 13 anatomical landmarks displayed on the orthogonal coordinate in Method-1 demonstrated that they spread out within the same region as the embryo enlarges and changes shape. The result indicated

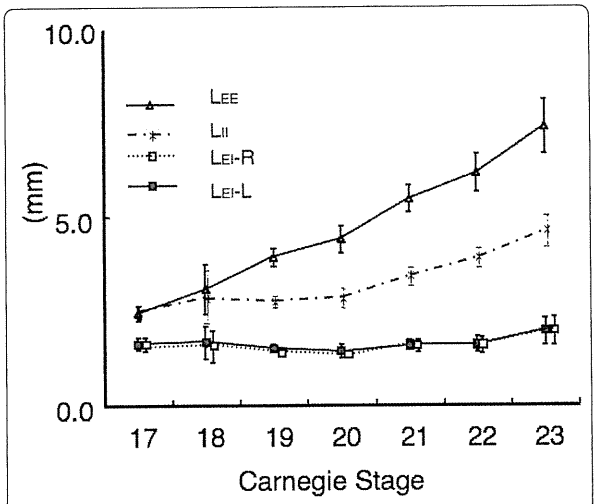

Figure 4 Distance between external and internal ears. Distances between bilateral external ears (L_{EE}), bilateral internal ears (L_{II}), and left internal and external ears (L_{EI}-L) and right internal and external ears (L_{EI} -R) are shown according to CS. (See also Figure 2C.) L_{EE} and L_{II} increase with development, whereas, L_{EI}-L and L_{EI} -R remain approximately constant between CS 17 and CS 23

that the positional changes that occur during the movement of the all anatomical landmarks including external and internal ears could be explained by differential growth.

The external ear did move mainly laterally, but not cranially. In the previous study, Streeter [11] had described that external ears gradually moved laterally and dorsally. As for cranial movement, Streeter suggested that the movement might be relative rather than real because the external ear is located at the side of the mouth during the development. Movement of the external ears along the dorsal/ventral axis was different from that of other anatomic landmarks such as the eyes, nose and mouth. The difference may result from the prominences they are derived from. Face components are formed from five facial primordia which appear early in the fourth week around the Mo [6-9,20,21]. Ey and Np were derived from the nasal prominence located cranial region of the Mo, while Ex1 and Ex6 were from the first and second pharyngeal arches respectively, which were located caudal region of the Mo.

In the present study the movement of the internal ear was limited in all directions. The internal ear develops from the otic placode that appears on either side of the

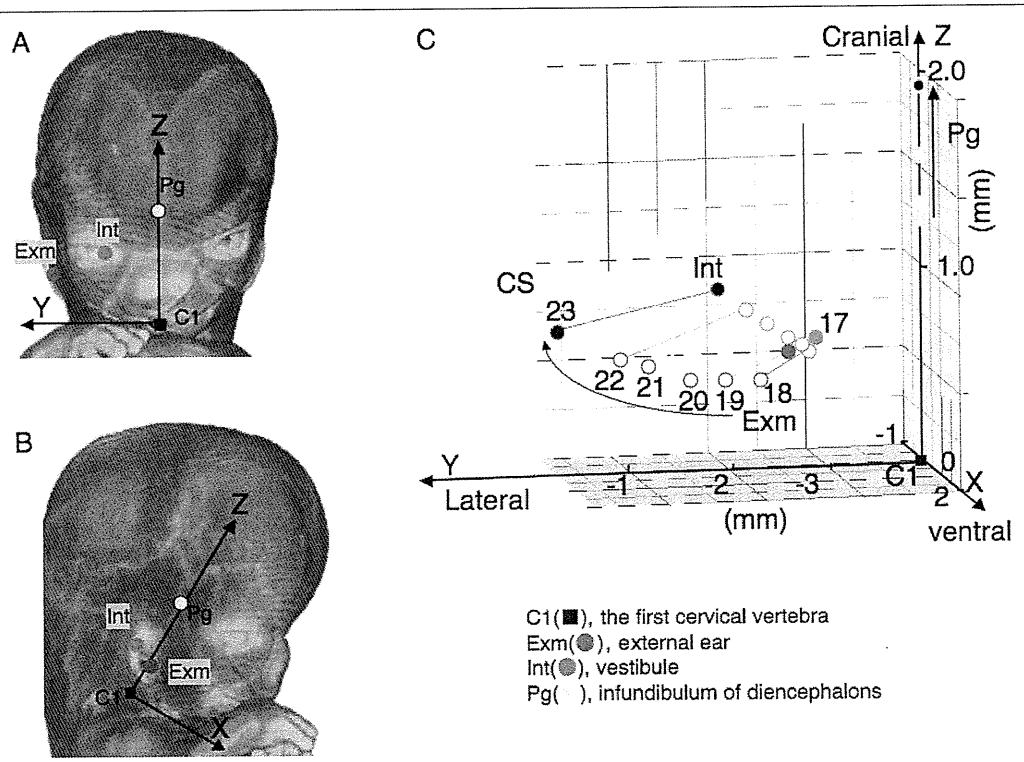

Figure 5 Relationship between right external and internal ears during development. Axes and anatomical landmarks are shown on frontal (A) and lateral (B) views of volume rendering images. (C) Three dimensional graph showing the relationship between right external and internal ears during development.

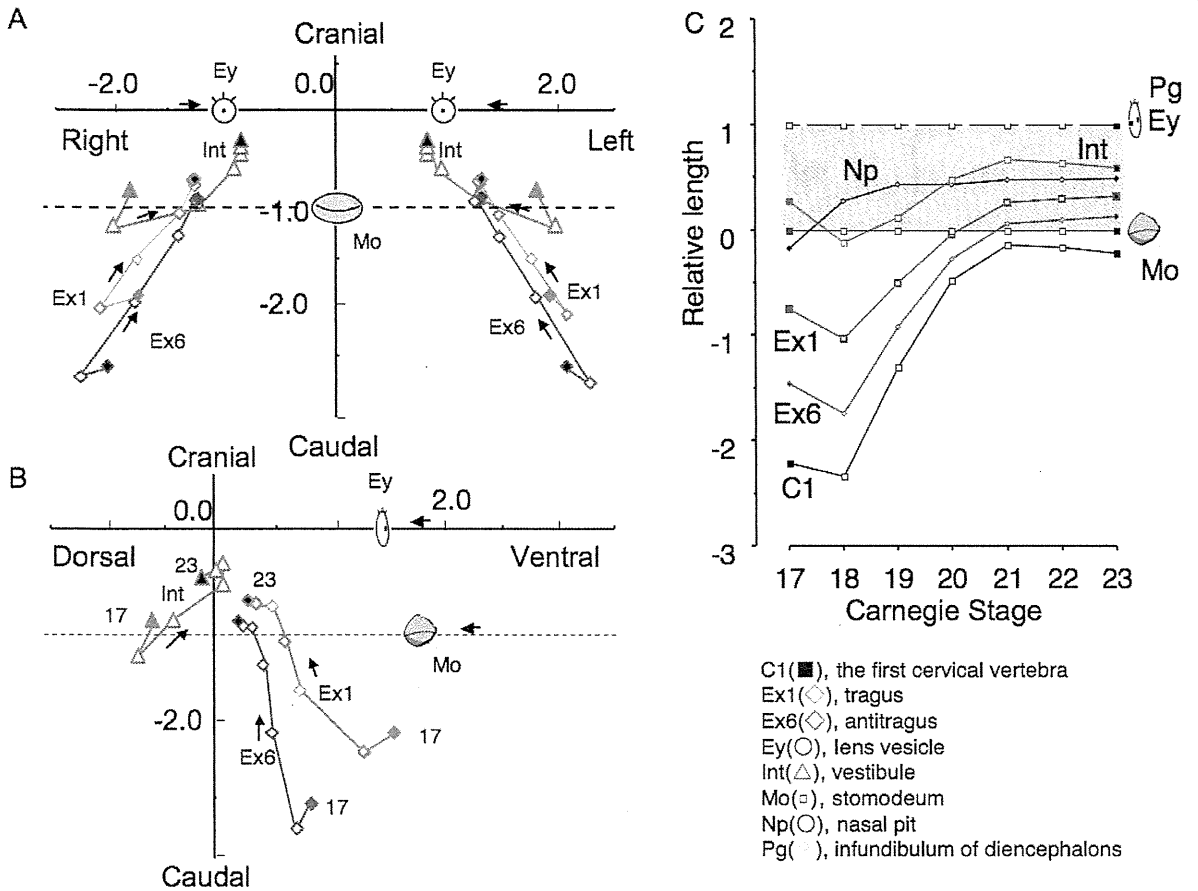

Figure 6 Movement of external and internal ear and anatomical landmarks during development in orthogonal coordinate defined in Method-2. Frontal (A) and left lateral (B) aspects of the face. Line connecting the middle point of the bilateral lens vesicle (Eys) and pituitary gland (Pg) was defined as reference axis (X-axis). The vertical line to the X-axis, which contained Stomodium (Mo) was defined as Z-axis of 3D orthogonal coordinate. The relative position of anatomical landmarks including Ex1, Ex6 and Int is compared with the distance between XY plane and Mo at each CS. (C) Movement of anatomical landmarks along the cranial/caudal (Z)-axis in the orthogonal coordinate in Method-2

neural tube at the level of the future hindbrain or metencephalon [1-4]. Sensory nucleoli of the vestibulocochlear complex are located close to the inner ear. Therefore, it seems hard to move the internal ear from the initial place. The distance between the external and internal ear was almost constant. This was anticipated, considering that all components of the ear relating to the sound-conducting apparatus of the middle and external ears and of the neurosensory structures of the internal ear develop simultaneously throughout development [5].

Surface reference point, i.e. Eys and Mo was adopted in Method-2 for comparison. To observe from the frontal position of the face in all stages, internal structure Pg was also selected. As expected, the movement in the orthogonal coordinate resembled our institutional macro-observation. The present data demonstrated the evident movement of the external ear from the ventral lateral caudal region to the region between the eyes and mouth.

Very different conclusions may be reached about movements of structures by selecting different references in the two methods. The difference may be owing to the following reasons:

1) The magnification of the embryo in all stages was identical in Method-1 while it was adjusted in Method-2. As a consequence, the relative position to the representative landmarks, Eys and Mo may be emphasized in Method-2. Undoubtedly, Eys and Mo are the most important landmarks to recognize the face and these are the landmarks by which the relative position of other landmarks was recognized.

2) There was a gross change of angle between the reference axes used between CS 17 and CS 23 (Figure 7). The change of angle may result from the formation of

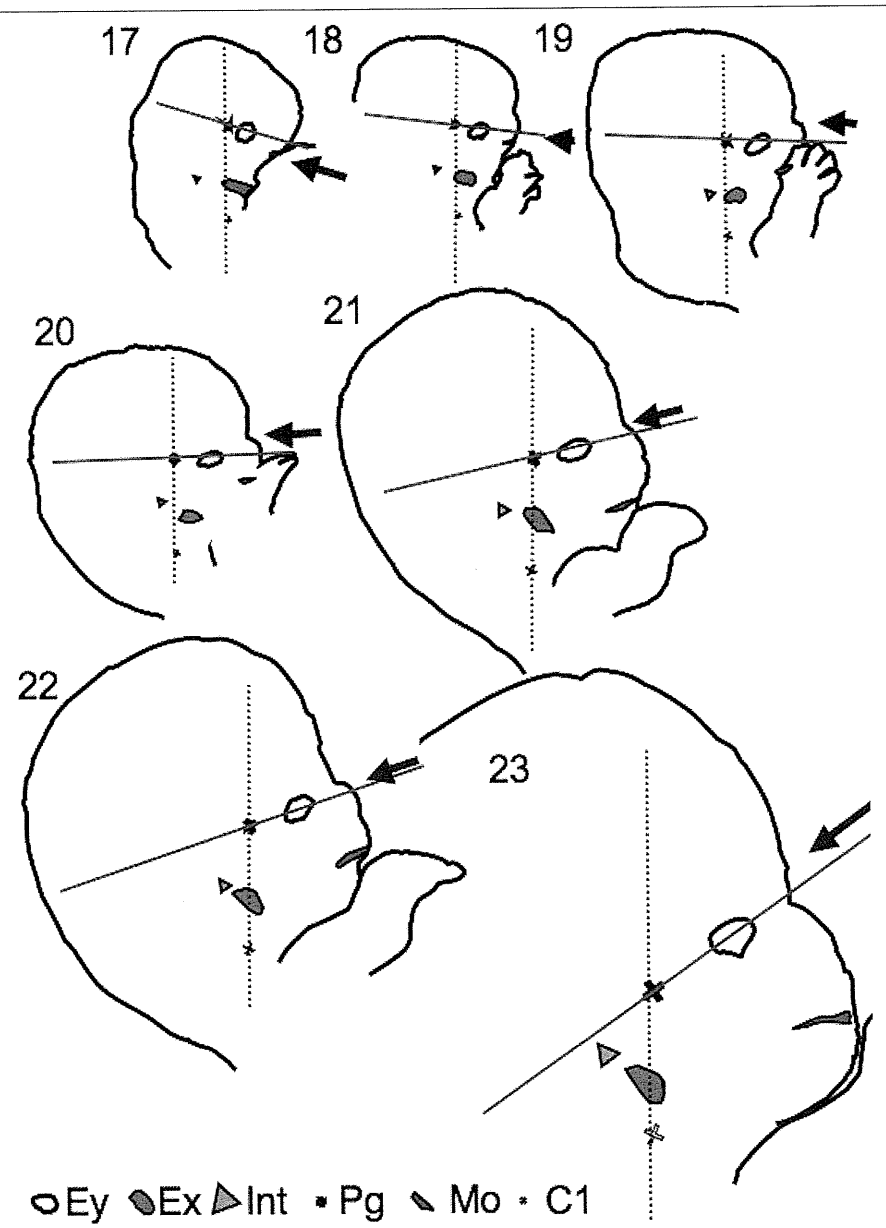

Figure 7 Lateral view of embryos between CS 17 and CS 23 showing craniofacial morphogenesis. The dashed line indicates the reference axis (Z-axis) in Method-1 and the red line indicates the reference axis (X-axis) in Method-2. The arrow indicates the frontal side of the face defined in Method-2. The following anatomical landmarks are drawn: external ear (Ex), internal ear (int), eye (Ey), mouth (Mo), pituitary gland (Pg), and first cervical vertebra (C1). Magnification is identical in all stages. The frontal position defined by Method-2 rotated as stages proceed. Note that both external and internal ears were located at similar positions between Pg and C1 between CS 17 and 23

the mandibular apparatus and the structures at the base of the skull as described in Streeter's study [11]. Pharyngeal arches, especially the first arch, play an important role in the formation of the face [1-5]. In addition to the external ear, many landmarks such as the maxilla, mandible, and a part of middle ear (the incus and malleus) are formed. The development of the mandibular apparatus may move the center of the face in the caudal direction, as well as push the external ear to the lateral side, as both are derived from first pharyngeal arches. Abnormal development of the components of the first pharyngeal arch results in various congenital anomalies of the face including mandible and ears [22]. The development of the structures at the base of the skull and its contents, i.

e. the brain, is another important factor resulting in the change of the angle. Chromosomal abnormalities, particularly trisomy 13 and trisomy 18 [22-25], are some congenital anomalies which show low-set ears. These syndromes express various symptoms including mental deficiency and small head and jaw. The abnormal development of the neurocranial structures in these cases may also affect the base of the skull, resulting in the symptoms of low-set ears as well.

Conclusions

The results indicate that movement of all anatomical landmarks, including external and internal ears, can be explained by differential growth. Also, when the external ear is recognized as one of the facial landmarks and having a relative position to other landmarks such as the eyes and mouth, the external ears seem to move cranially.

Abbreviations

(3D): Three-dimensional; (2D): Two-dimensional; (CS): Carnegie Stages; (Ex1): Tragus; (Ex6): Antitragus; (Int): Vestibule; (Mo): Stomodeum; (Np): Nasal pit; (Ey): Lens vesicle; (Pg): Infundibulum of diencephalons; (C1): Cranial region of the first cervical vertebra; (L_{EE}): Distance between bilateral Ex1s; (L_{EI}): Distance between collateral Ex1 and Int; (Exm): The middle point of antitragus and tragus

Acknowledgements

I am deeply indebted to the Executive Vice President of Kyoto University, Kohei Shiota for providing us the invaluable MR data. I also acknowledge the contribution of collaborating obstetricians and the previous members of the Congenital Anomaly Research Center, Kyoto University Graduate School of Medicine. This study was supported by the Grants #228073, #238058, #21790810 and #22591199 from the Japan Society for the Promotion of Science (JSPS) and the Japan Science and Technology (JST) institute for Bioinformatics Research and Development (BIRD).

Author details

[1]Human Health Science, Graduate School of Medicine, Kyoto University, 606-8507, Sakyo-ku Shogoin Kawahara-cyo 53, Kyoto, Japan. [2]Congenital Anomaly Research Center, Kyoto University Graduate School of Medicine, Kyoto, 606-8507, Japan. [3]Institute of Applied Physics, University of Tsukuba, Ibaragi, 305-8573, Japan.

Authors' contributions

MK has made substantial contributions to conception and design, acquisition of data, and statistic analysis. SY have been involved in drafting the manuscript or revising it critically for important intellectual content. CU has made substantial contributions to acquisition of data and maintenance of the human embryos specimen. KK have made substantial contributions to acquisition of data especially MR imaging. TT has made substantial contributions to conception and design and general supervision of the research group. All authors read and approved the final manuscript.

Competing interests

The authors declare that they have no competing interests.

Received: 11 August 2011 Accepted: 1 February 2012
Published: 1 February 2012

References

1. Drews U: **Auditory and Vestibular organ.** In *Color Atlas of Embryology.* Edited by: Drews U. New York: Thieme Medical Publishers; 1995:274-279.
2. Moore KL, Persaud TVN: **The Eye and Ear.** In *The Developing Human: Clinically Oriented Embryology.*. 8 edition. Edited by: Moore KL, Persaud TVN. Philadelphia: Saunders; 2008:419-438.
3. Sadler TW: **Ear.** In *Langman's medical embryology.*. 11 edition. Edited by: Sadler TW. Philadelphia: Walters Kluwer Health/Lippincott William 2010:327-334.
4. Schoenwolf GC, Bleyl SB, Brauer PR, Francis-West PH: **Development of the Ears and Eyes.** In *Larsen's human embryology.*. 4 edition. Edited by: Schoenwolf GC, Bleyl SB, Brauer PR, Francis-West PH. Philadelphia: Churchill Livingstone/Elsevier; 2009:583-616.
5. Giraldez F, Fritzsch B: **The molecular biology of ear development - "Twenty years are nothing".** *Int J Dev Biol* 2007, **51**:429-438.
6. Drews U: **Head.** In *Color Atlas of Embryology.* Edited by: Drews U. New York: Thieme Medical Publishers; 1995:346-357.
7. Moore KL, Persaud TVN, Torchia MG: **The pharyngeal apparatus.** In *The developing human: clinically oriented embryology.*. 8 edition. Edited by: Moore KL, Persaud TVN. Philadelphia, PA: Saunders/Elsevier; 2008:159-196.
8. Sadler TW, Langman J: **Head and Neck.** In *Langman's medical embryology.*. 11 edition. Edited by: Sadler TW. Philadelphia: Wolters Kluwer Lippincott Williams 2010:265-292.
9. Schoenwolf GC, Bleyl SB, Brauer PR, Francis-West PH: **Development of the pharyngeal apparatus and face.** In *Larsen's human embryology.*. 4 edition. Edited by: Schoenwolf GC, Bleyl SB, Brauer PR, Francis-West PH. Philadelphia, PA: Elsevier/Churchill Livingstone; 2009:543-582.
10. O'Rahilly R, Müller F: *Developmental stages in human embryos: including a revision of Streeter's Horizons and a survey of the Carnegie Collectio* Washington, D.C.: Carnegie Institution of Washington; 1987.
11. Streeter GL: **Development of the auricle in the human embryo.** *Contrib Embryol Carnegie Inst* 1922, **14**:111-138.
12. Gasser RT: **Evidence that some events of mammalian embryogenesis can result from differential growth, making migration unnecessary.** *Anat Rec B* 2006, **289B**:53-63.
13. Shiota K, Yamada S, Nakatsu-Komatsu T, Uwabe C, Kose K, Matsuda Y, Haishi T, Mizuta S, Matsuda T: **Visualization of human prenatal development by magnetic resonance imaging (MRI).** *Am J Med Genet A* 2007, **143A**:3121-3126.
14. Nishimura H, Takano K, Tanimura T, Yasuda M: **Normal and abnormal development of human embryos: first report of the analysis of 1,213 intact embryos.** *Teratology* 1968, **1**:281-290.
15. Yamada S, Uwabe C, Fujii S, Shiota K: **Phenotypic variability in human embryonic holoprosencephaly in the Kyoto Collection.** *Birth Defects Res A Clin Mol Teratol* 2004, **70**:495-508.
16. Kameda T, Yamada S, Uwabe C, Suganuma N: **Digitization of clinical and epidemiological data from the Kyoto Collection of Human Embryos: maternal risk factors and embryonic malformations.** *Cong Anom* .
17. Matsuda Y, Utsuzawa S, Kurimoto T, Haishi T, Yamazaki Y, Kose K, Anno I, Marutani M: **Super-parallel MR microscope.** *Magn Reson Med* 2003, **50**:183-189.
18. Matsuda Y, Ono S, Otake Y, Handa S, Kose K, Haishi T, Yamada S, Uwabe C, Shiota K: **Imaging of a large collection of human embryo using a super-parallel MR microscope.** *Magn Reson Med Sci* 2007, **6**:139-146.
19. Gleiberman AS, Fedtsova NG, Rosenfeld MG: **Tissue interactions in the induction of anterior pituitary: role of the ventral diencephalon, mesenchyme, and notochord.** *Dev Biol* 1999, **213**:340-353.
20. Chai Y, Maxson RE: **Recent advances in craniofacial morphogenesis.** *Dev Dyn* 2006, **235**:2353-2375.
21. Gitton Y, Heude E, Vieux-Rochas M, Benouaiche L, Fontaine A, Sato T, Kurihara Y, Kurihara H, Couly G, Levi G: **Evolving maps in craniofacial development.** *Semin Cell Dev Biol* 2010, **21**:301-308.
22. Passos-Bueno MR, Ornelas CC, Fanganiello RD: **Syndromes of the first and second pharyngeal arches: A review.** *Am J Med Genet A* 2009, **149A**:1853-1859.
23. Hall JG: **Handbook of physical measurement.** Oxford; New York: Oxford University Press;, 2 2007.
24. Feingold M, Bossert WH: **Normal values for selected physical parameters: an aid to syndrome delineation.** *Birth Defects Orig Artic Ser* 1974, **10**:1-16.
25. Hunter A, Frias JL, Gillessen-Kaesbach G, Hughes H, Jones KL, Wilson L: **Elements of morphology: standard terminology for the ear.** *Am J Med Genet A* 2009, **149A**:40-60.

doi:10.1186/1746-160X-8-2
Cite this article as: Kagurasho *et al.*: Movement of the external ear in human embryo. *Head & Face Medicine* 2012 **8**:2.

Efficient generation of transgene-free human induced pluripotent stem cells (iPSCs) by temperature-sensitive Sendai virus vectors

Hiroshi Ban[a,1], Naoki Nishishita[b,c,1], Noemi Fusaki[a,d,2], Toshiaki Tabata[a], Koichi Saeki[a], Masayuki Shikamura[c], Nozomi Takada[c], Makoto Inoue[a], Mamoru Hasegawa[a], Shin Kawamata[b,c,2], and Shin-Ichi Nishikawa[b,c]

[a]DNAVEC Corporation, Tsukuba, Ibaraki 300-2611, Japan; [b]RIKEN Center for Developmental Biology, Kobe, Hyogo 650-0047, Japan; [c]Foundation for Biomedical Research and Innovation, Kobe, Hyogo 650-0043, Japan; and [d]Precursory Research for Embryonic Science and Technology, Japan Science and Technology Agency, Kawaguchi, Saitama 332-0012, Japan

Edited by Yuet Wai Kan, University of California San Francisco School of Medicine, San Francisco, CA, and approved July 7, 2011 (received for review March 21, 2011)

After the first report of induced pluripotent stem cells (iPSCs), considerable efforts have been made to develop more efficient methods for generating iPSCs without foreign gene insertions. Here we show that Sendai virus vector, an RNA virus vector that carries no risk of integrating into the host genome, is a practical solution for the efficient generation of safer iPSCs. We improved the Sendai virus vectors by introducing temperature-sensitive mutations so that the vectors could be easily removed at non-permissive temperatures. Using these vectors enabled the efficient production of viral/factor-free iPSCs from both human fibroblasts and CD34$^+$ cord blood cells. Temperature-shift treatment was more effective in eliminating remaining viral vector-related genes. The resulting iPSCs expressed human embryonic stem cell markers and exhibited pluripotency. We suggest that generation of transgene-free iPSCs from cord blood cells should be an important step in providing allogeneic iPSC-derived therapy in the future.

regenerative medicine | nonintegrating RNA vector

Safer and more efficient reprogramming methods have been explored since the first report of the generation of human induced pluripotent stem cells (iPSCs) (1, 2). Toward this end, several techniques have been used for obtaining integration and/or transgene-free iPSCs, including the use of plasmids (3, 4), the Cre/loxP system (5, 6), adenoviruses (7), piggyBac (8, 9), minicircle vector (10), and proteins (11, 12). However, these methods suffer from low efficiency, require repetitive induction, and/or produce insufficient excision of integrated vectors. Synthetic modified mRNA may solve the problem, but the reagents must be added every day (13). Thus, more efficient and simple methods are needed to generate human iPSCs with no noise of integration or remaining factors for both clinical applications and basic studies.

An alternative technology involves the use of Sendai virus (SeV) vectors. SeV, a member of the *Paramyxovirdae* family, is an enveloped virus with a single-stranded, negative-sense, nonsegmented RNA genome of ~15 kb (14). Importantly, recombinant SeV vectors replicate only in the cytoplasm of infected cells and do not go through a DNA phase or integrate into the host genome (15). SeV vectors have proven to be efficient for the introduction of foreign genes in a wide spectrum of host cell species and tissues, and SeV vectors have been studied for applying to clinical studies of gene therapy for cystic fibrosis, critical limb ischemia, vaccines for AIDS, and other areas (reviewed in ref. 16). We previously reported that the SeV vectors efficiently generate human iPSCs from human fibroblasts (17) and human blood cells (18). However, to apply SeV vector technology to the generation of safer iPSCs, the issue of the sustained cytoplasmic replication of viral vectors after the iPSCs have been established had to be overcome, even though viral vectors are slowly diluted during the robust cell division of iPSCs and SeV vector–positive cells can be removed using an anti–SeV-HN antibody (17). In other words, a more efficient shutdown of viral replication is needed to generate human iPSCs. We considered the use of temperature-sensitive (TS) SeV vectors the likeliest best solution.

Here we show that by introducing point mutations in the polymerase-related genes, we obtained new TS vectors and efficiently generated viral/factor-free human iPSCs from fibroblasts using these vectors by two strategies, (*i*) replacing the MYC vector only and (*ii*) replacing all reprogramming vectors to the TS vectors. We also applied this method to CD34$^+$ cord blood (CB) cells because SeV vector provides a highly efficient gene transfer into human CB-derived hematopoietic stem cells (19). CD34$^+$ CB cells are the youngest somatic stem cells and are expected to have no postnatal genomic aberration by irritants from the environment or UV rays. They correspond to the hematopoietic stem cells and progenitors with less epigenetic modification related to hematopoietic differentiation. These unique features of CD34$^+$ CB cells suggest that this cell fraction might be an ideal cell source fraction for generating a gold standard iPSC. However, the risk of foreign gene integration (20, 21) needs to be overcome for future clinical applications. We successfully obtained viral/factor-free CB-iPSCs by the TS SeV vectors, and examined the advantages of using the TS SeV vector.

Results

Generation of TS SeV Vectors. The SeV RNA polymerase comprises the phosphoprotein (P) and the large protein (L), and formation of the P-L complex is required for RNA synthesis (14). Mutations in P or L have been shown to confer temperature sensitivity to the virus (22, 23). Although a conventional nontransmissible F protein-deficient (ΔF)/TS vector was demonstrated to have low cytotoxicity at temperatures above 37 °C (24), it still expressed the *GFP* gene at 39 °C, albeit at slightly lower levels (Fig. 1*B*). Thus, we generated a greater number of TS vectors using combination of known point mutations in the *P* and/or *L* genes and screened for *GFP* gene expression in infected cells

Author contributions: N.N., N.F., S.K., and S.-I.N. designed research; H.B., N.N., N.F., M.S., N.T., and S.K. performed research; N.F., T.T., K.S., M.I., M.H., S.K., and S.-I.N. analyzed data; and N.F. and S.K. wrote the paper.

Conflict of interest statement: H.B., T.T., K.S., M.I., and N.F. are employees of DNAVEC Corporation. M.H. is a founder of DNAVEC Corporation.

This article is a PNAS Direct Submission.

Freely available online through the PNAS open access option.

Data deposition: The data reported in this paper have been deposited in the Gene Expression Omnibus (GEO) database, www.ncbi.nlm.nih.gov/geo (accession nos. GSE24240 and GSE25090).

[1]H.B. and N.N. contributed equally to this work.

[2]To whom correspondence may be addressed. E-mail: nfusaki@dnavec-corp.com or kawamata@cdb.riken.jp.

This article contains supporting information online at www.pnas.org/lookup/suppl/doi:10.1073/pnas.1103509108/-/DCSupplemental.

at various temperatures. The TS vectors obtained were (*i*) P2 vectors (D433A, R434A, and K437A), which contain a charge-to-alanine mutation in the L-binding domain of the P protein (22); (*ii*) TS7 vectors (Y942H, L1361C, and L1558I); (*iii*) TS13 vectors (P2 and L1558I); and (*iv*) TS15 vectors (P2, L1361C, and L1558I), as indicated in Fig. 1. In the present study, we chose to evaluate these candidate vectors with combined mutations, because a single mutation appeared to be insufficient to confer temperature sensitivity (i.e., the Y942H, L1558I, or L1361C vector). Furthermore, by using TS candidates with combined mutations, the occurrence of WT revertant, as occasionally observed in RNA viruses (14), was less likely. In contrast with the conventional SeV vector, the TS7 and TS13 vectors expressed *GFP* at 32 °C and 35 °C, and weakly at 37 °C, but not at nonpermissive temperatures of 38 °C or 39 °C. The TS15 vector exhibited greater temperature sensitivity; with this vector, *GFP* expression was barely detected at 37 °C (Fig. 1*B*). We confirmed that there was no *GFP* expression after transfection of cells with the TS7 and TS13 vectors after temperature-shift treatment to 39 °C, even when the infected cells were then cultured at 37 °C for >1 mo with several passages (Fig. 1*C*). None of the vectors was cytotoxic, and all infected cells were attached and live, with or without temperature-shift treatment. Thus, we used these TS vectors to generate human iPSCs.

Generation of Human iPSCs with TS SeV Vectors from Fibroblasts. To apply the TS vectors to generate human iPSCs, we adopted two strategies, (*i*) to replace only *c-MYC*–carrying vector and (*ii*) to replace all of the four gene-carrying SeV vector mixtures to the TS vectors. Our previous study showed that the exogenous *c-MYC* inserted between the *HN* and *L* positions in the SeV vector (*HNL-MYC*) persisted in the infected cells longer than any other vectors carrying *OCT3/4, SOX2*, or *KLF4* at the top of the vectors (18+). When *c-MYC* was inserted at the 18+ position, such selective retention of the c-*MYC*–carrying vector was not observed. This was apparently due to the prolonged replication of the *HNL-MYC* vector (17). Because GFP expression with the TS vectors was relatively weak compared with that obtained using conventional vectors (Fig. 1*B*), we initially inserted *HNL-MYC* into the TS vectors so that the initial levels of expression could be restored by the polymerases supplied in trans from the other vectors (*OCT3/4*, *KLF4*, and *SOX2*). In addition, it was hoped that by using this strategy, the viral vectors might easily disappear when the remaining vector was *HNL-MYC* in the TS vector alone (Fig. 2*A*). Using these vectors at a multiplicity of infection (MOI) of 3, we obtained colonies from human fibroblast cells that were alkaline phosphatase (ALP)-positive and exhibited human embryonic stem (ES) cell-like morphology ~28 d after induction (Fig. 2*B* and Table S1). We then monitored the amount of the SeV genome present during reprogramming and cell expansion using quantitative RT-PCR (qRT-PCR). Surprisingly, replacement of the *HNL-MYC* vector into only one of the four reprogramming factor mixtures using the TS vectors resulted in a marked decrease in all viral genomes after the appearance of the iPSCs (Fig. 2*C*). As expected, expression of *c-MYC* on the TS vectors was correlated with the viral genome (Fig. S1). Then individual colonies were isolated, and the remaining SeV genome in each colony was evaluated. During cell expansion, the vectors were diluted, and most colonies were only partially positive for SeV (Fig. 2*D*, *Middle*). At passage 4, 80% of the colonies were negative for the viral genome using the TS13-

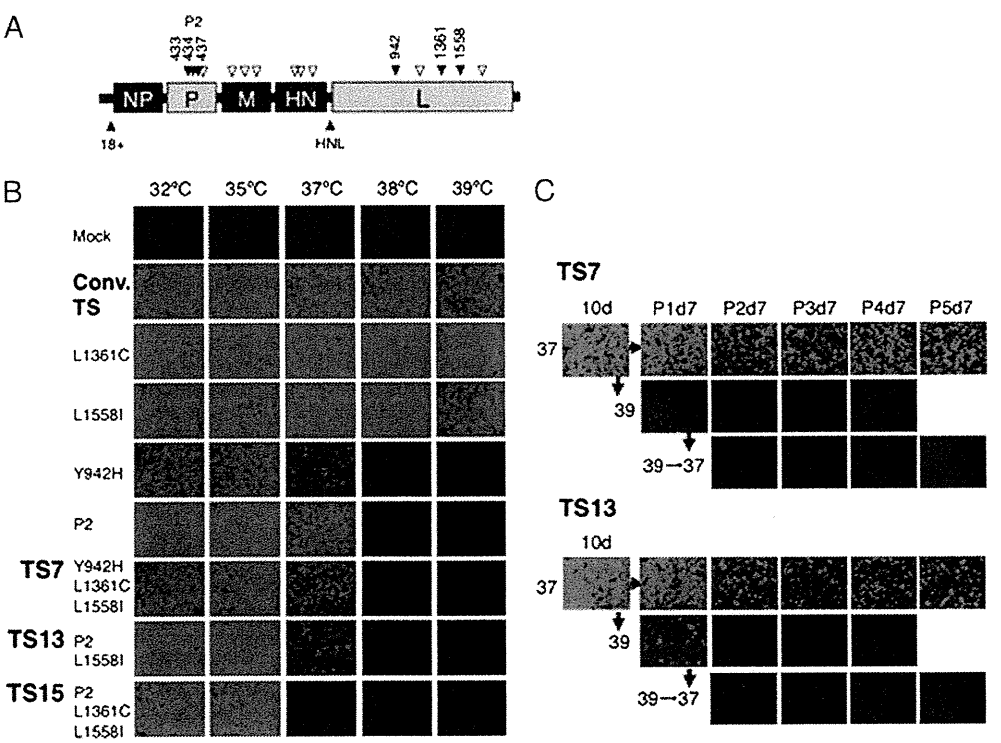

Fig. 1. Generation of TS SeV vectors and inactivation after temperature-shift treatment. (*A*) Point mutations were introduced into the polymerase-related genes *P* (P2: 433, 434, and 437) and/or *L* (942, 1361, and 1558), as indicated in the schematic structure of the ΔF/SeV vector. Open angles indicate conventional mutations in the previous TS vector; closed angles, newly introduced mutations. (*B*) Confluent LLC-MK2 cells were transduced with each SeV vector carrying *GFP* at an MOI of 5 and cultured at the indicated temperatures (32, 35, 37, 38, and 39 °C). Green fluorescence was compared at 3 d after infection. (*C*) To confirm the irreversible inactivation of gene expression by temperature-shift treatment, infected cells were cultured at 37 °C for 10 d and then split into two groups, one group cultured at 37 °C and the other cultured at 39 °C for 28 d, with cells passaged every 7 d. Similarly, cells infected with a TS vector treated at a nonpermissive temperature of 39 °C for 7 d were also cultured for a further 28 d at 37 °C, with cells passaged every 7 d, to evaluate *GFP* expression.

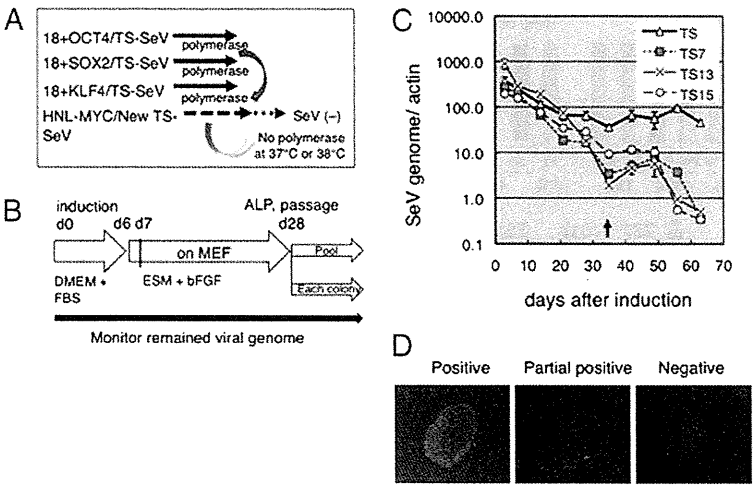

Fig. 2. (*A*) Strategy used to obtain vector/factor-free iPSCs with an SeV vector mixture. Human fibroblasts were infected with the SeV vector mixture containing four factors. During reprogramming, polymerases may be supplied to the TS vector (which has *c-MYC* at the HNL position) by *OCT3/4-*, *SOX2-*, and *KLF4*-carrying conventional SeV vectors. Then the SeV vector may disappear when there is TS vector alone at nonpermissive temperature. (*B*) Procedure for reprogramming using SeV vectors. (*C*) qRT-PCR of existing SeV genomes in induced cells. RNA was extracted from cells between 3 d and 2 mo after infection, and the amount of SeV genome was analyzed by qRT-PCR. iPSC colonies were passaged every 7 d after day 35 (arrow), and whole colonies on the culture dish were analyzed. (*D*) Typical staining of iPSC colonies with anti-SeV antibodies. (*Left*) At passage (P) 1, many colonies were positive for SeV. (*Middle*) After several passages (P4), many colonies were partially positive. (*Right*) Colonies were found to be negative for SeV at P10. (Scale bar: 200 μm.)

HNL-MYC and TS15-*HNL-MYC* vectors, and by passage 10, all colonies were negative for the vector by qRT-PCR (Fig. 3*A*, *Left*). Because the number of SeV-negative colonies was not increased using the TS7 vector at passage 10, although the partial negative colonies were increased, the iPSCs were subjected to a temperature shift to 38 °C (Fig. 3*A*, *Right*). Incubation of cells at 38 °C for 3–5 d was sufficient to obtain SeV-negative iPSCs (Figs. 3*A* and 4*B*) with no changes in the expression of human ES cell (hESC) marker genes, *NANOG* (Fig. 4*B*), or the other related marker genes. Quantitative RT-PCR analysis and Western blot analysis of these iPSCs obtained by the first strategy revealed no detectable viral genome or protein expression in the established iPSCs at the late passage numbers, with slightly detectable viral genome or protein expression in the pooled colonies at passage 8 (1/1,000–1/10,000 compared with day 3; Fig. 3 *B* and *C* and Table S3). TS15 showed higher dilution than other vectors, comparable to their temperature sensitivities. More importantly, copy numbers of *OCT3/4, SOX2, KLF4*, and *c-MYC* genes in SeV-generated iPSCs were the same as in parental cells, in contrast to retroviral-generated iPSCs, in which copy numbers were verified because of the vector integration (Fig. 3*D*). The condition and the efficiencies of these experiments and characteristics of obtained iPS clones are summarized in Tables S1 and S3.

Expression of Human ES Cell Markers and Epigenetics. All iPSCs examined expressed hESC markers, as determined by qRT-PCR, and were positive for stage-specific embryonic antigen (SSEA)-4, TRA-1-60, TRA-1-81, NANOG, and OCT4, as demonstrated by immunostaining (Fig. S2 *A* and *B*). Furthermore, CpG dinucleotides at the *OCT3/4* promoter region in the iPSCs were demethylated (Fig. S2*C*). Global gene expression in the iPSCs was similar to that of hESCs (Fig. S3*A*). Clustering analysis revealed a high degree of similarity among the reprogrammed iPSCs obtained using the TS7, TS13, or TS15 vectors that clustered together with hESCs and was distant from that of the parental somatic cells. These iPSCs had a normal 46 XY or 46 XX karyotype, even after temperature-shift treatment, and could be maintained for more than 20 passages (Fig. S4*A* and Table S3). DNA fingerprinting analysis verified that these iPSCs were indeed derived from the parental fibroblast cells (Fig. S4*B*).

Established iPSCs Show Potentiality of Differentiation to Three Germ Layers. The ability of hESCs/iPSCs to differentiate into all cell types provides the basis for their potential in regenerative medicine. Thus, we investigated the differentiating potential of SeV-generated iPSCs by evaluating teratoma formation. In these experiments, the virus-negative iPSCs were injected s.c. or i.m. into NOD/SCID mice. Histological examination of the teratomas revealed that the tissues had originated from the three embryonic germ layers and included neural and epithelial tissues, muscle, cartilage, bone, gut-like structures, and various glandular structures (Fig. S3*B*). We further tested the pluripotency of SeV-generated iPSCs in vitro. Like hESCs, these iPSCs formed embryoid bodies in suspension culture (Fig. S4*C*). For mesoderm-derived differentiation, the embryoid bodies were grown in adherent culture with 0.1 mM ascorbic acid and 20% FBS to enhance cardiomyocyte differentiation (25), whereas an established protocol for hESCs involving activin A treatment (26) was used for the induction of definitive endoderm cells. As a result, SeV-generated iPSCs differentiated into beating cardiomyocytes and endoderm-derived pancreatic cells that stained positive for pancreatic and duodenal homeobox 1 (PDX1; Fig. S4*C*). Coculture of these iPSCs with PA6 feeder cells resulted in the generation of dopaminergic neurons (ectoderm derivatives) that were positive for βIII tubulin and tyrosine hydroxylase (27) (Fig. S4*C*). These data indicate that the SeV-generated iPSCs are pluripotent, like hESCs, and respond to different differentiation stimuli. Based on these results, we conclude that the viral/factor-free iPSCs generated using TS SeV vectors meet the criteria of hESCs and could serve as a clinically important source of stem cells without the danger of integration of any foreign genes.

Generation of Human iPSCs from CB Cells. In the second strategy, we obtained viral-free iPSCs from human fibroblasts using TS13 or TS7 vector mixtures consisting of four reprogramming factors (i.e., 4F/TS13 and 4F/TS7, respectively) at a higher MOI of 30 at 37 °C, with (TS7) or without (TS13) temperature-shift treatment (Fig. 4 *A* and *B* and Table S1). In this case, we used a higher MOI because we could not obtain iPSCs at a lower MOI, likely due to the weak expression of TS vectors at 37 °C, lacking any supplemental polymerases from mixed conventional vectors. However,

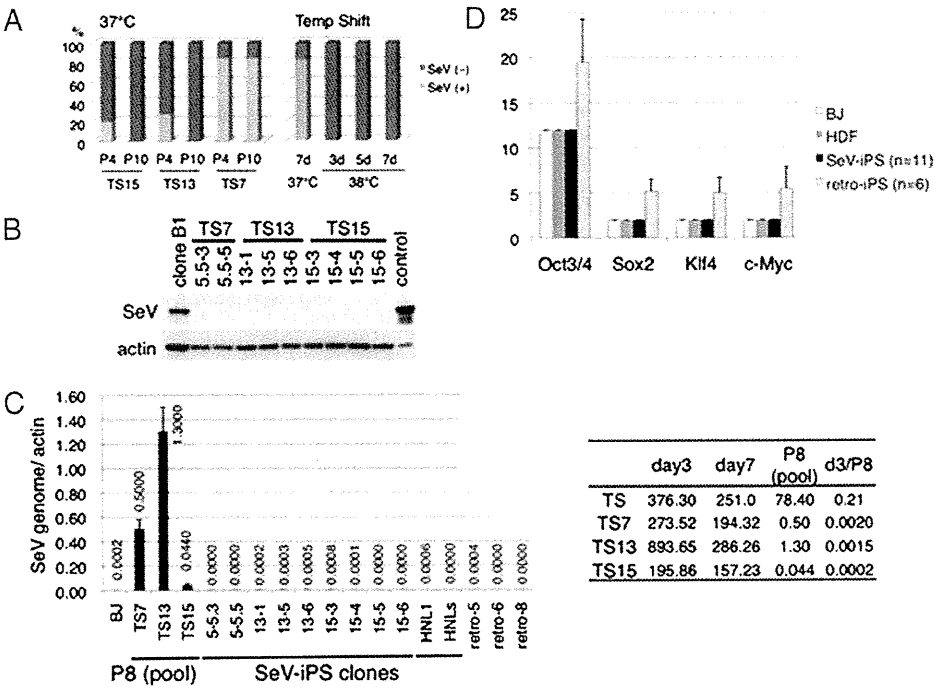

	day3	day7	P8 (pool)	d3/P8
TS	376.30	251.0	78.40	0.21
TS7	273.52	194.32	0.50	0.0020
TS13	893.65	286.26	1.30	0.0015
TS15	195.86	157.23	0.044	0.0002

Fig. 3. (*A*) Ratio of SeV-positive colonies. P, passage number. (*Left*) Randomly chosen colonies were expanded independently, and the existence of SeV vectors was evaluated by qRT-PCR at P4 and P10. The number of positive and negative colonies was counted and is expressed for each as a ratio of all colonies chosen (n = 12 per each TS vector). (*Right*) Temperature shift to a nonpermissive temperature of 38 °C effectively removed SeV vectors from the iPSC colonies generated using TS7 vectors. The culture dishes at P4 were split and transferred to culture at 37 or 38 °C for the number of days indicated. The ratio was calculated as left panel. (*B*) SeV proteins were not detected in iPSC colonies by Western blot analysis with anti-SeV antibodies. Clone B1, positive control for iPSCs in which the SeV persisted (17); control, LLC-MK2 cells transfected with plasmids encoding SeV vectors. 5.5-3 and 5.5-5 were generated with MYC/TS7; 13-1, 13-5, and 13-6 were generated with MYC/TS13; and 15-3, 15-4, 15-5, and 15-6 were generated with MYC/TS15. (*C*) qRT-PCR of viral genome in SeV-generated iPSCs (viral genome/actin). BJ, parental fibroblasts; day 3 and day 7, BJ cells infected with SeV vectors after 3 and 7 d; HNL1 and HNLs, iPSCs established using conventional SeV (17). P8, pooled colonies at passage 8. Values <0.001 were backgrounds under the calculation curve as detected in parental cells. (*D*) Copy numbers of *OCT3/4*, *SOX2*, *KLF4*, and *c-MYC* in parental cells [BJ and human dermal fibroblast (HDF) cells] and iPSCs generated by SeV (SeV-iPS; n = 11) or retrovirus (retro-iPS; n = 6), as determined by qRT-PCR of genomic DNA. The passage numbers of tested clones are listed in Table S3.

an MOI of only 2 was sufficient to generate iPSCs from the CB cells described below, possibly because of the highly efficient gene transfer into human CB stem cells (19). We infected freshly isolated mononuclear cells with the GFP construct at an MOI of 2 and found that GFP expression was limited to the $CD34^+$ fraction (43% of the $CD34^+$ cells were GFP^+ cells), whereas no GFP^+ cells were found in the $CD34^-$ fraction at 2 d after SeV infection (19). The rate of SeV infection determined by GFP expression in $CD34^+$ cells was increased up to 100% if we used SeV vectors at an MOI of 20. This fraction corresponds to hematopoietic stem cells or progenitors, as reported elsewhere (28). Then freshly isolated purified $CD34^+$ CB cells (purity of $CD34^+$, 96–99%) or the frozen $CD34^+$ CB cells (RIKEN BioResource Center; purity of $CD34^+$, 97–99%), thawed 1 d before infection, were used for SeV infection. These cells were treated with a SeV vector mixture consisting of SeV TS7-*OCT3/4*, -*SOX2*, -*KLF4*, and -*c-MYC*. Infected cells were incubated under hematopoietic cell culture conditions, followed by cocultivation on mitomycin C (MMC)-treated SNL cells on day 4 or day 10 (Fig. 4*C*). hESC-like colonies expressing SSEA-4 appeared after 14 d of cocultivation with SNL (18 d after SeV infection), whereas no colonies were obtained after transfer onto SNL on day 10 (Table S2). The efficiency with which iPSC colonies emerged on SNL feeder cells using SeV TS7 vectors is also shown in Table S2. To eliminate remaining SeV virus constructs, ESC-like colonies were subjected to heat treatment at 38 °C for 3 d and recloned. SeV-positive cells constituted 60–80% of total cells within hESC-like colonies before heat treatment (clones SeV iPSC 4, 15, and 17; passage 2). This was reduced to 0% after recloning (clones SeV iPSC 4A, 15A, and 17A; passage 4), followed by the heat treatment. The percentages of SeV-positive cells were determined by the proportion of sum of the area positively detected with anti-SeV HN (envelope) antibody against total colony area. In the agreement with this staining result, SeV constructs were not detected by qRT-PCR at passage 4 after heat treatment (Fig. 4*E*). The virus-negative ESC-like clones showed the expression of hESC markers (Fig. S5 *A* and *B*), global gene expression profile similar to that of hESCs (Fig. S5 *C* and *E*), and normal karyotype (Fig. S5*D*). Seven established cell clones were tested for embryoid body–mediated in vitro differentiation potential, and three out of the seven clones were found to have in vivo differentiation potential in a teratoma formation assay with SCID mice. All three of these clones were able to give rise to cells of all three germ layers as detected by immunocytochemistry and cell morphology studies (Fig. S5*F*). These three lines formed the teratomas with a cystic mass containing differentiated tissues morphologically corresponding to all three germ layers (Fig. S5*F*). The characterization of established clones from fibroblasts and CB cells is summarized in Table S3.

Discussion

The present study has demonstrated that the established TS SeV vectors TS15, TS13, and TS7 are highly effective tools with which we were able to obtain transgene-free human iPSCs. These iPSCs were generated efficiently by robust gene replication, with a subsequent rapid decrease in the level of factor-carrying SeV vectors

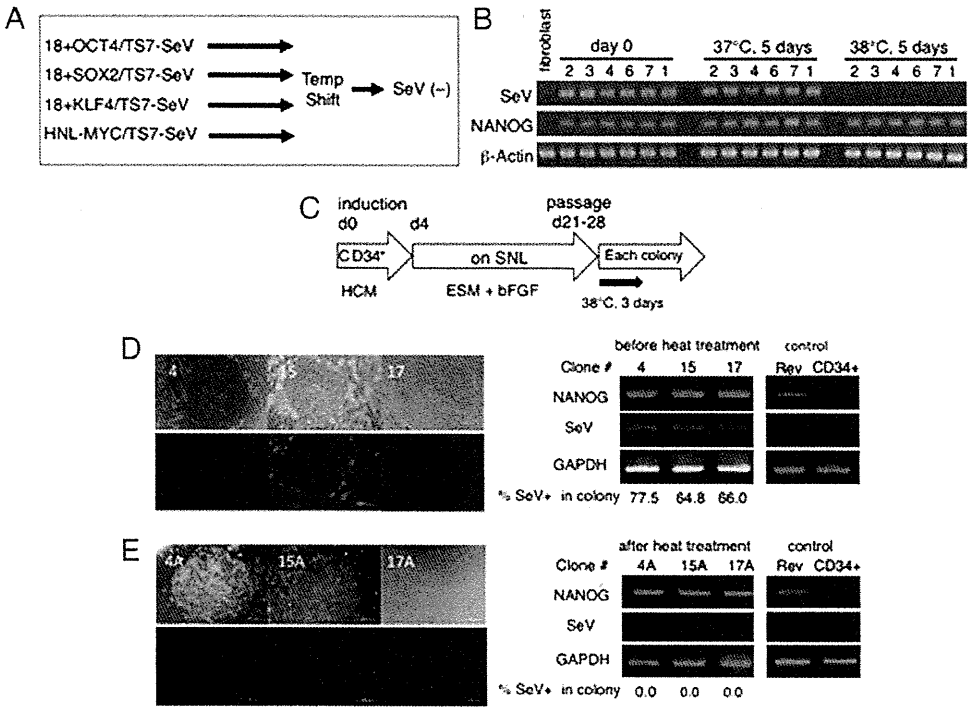

Fig. 4. Our second strategy with temperature-shift treatment. (*A*) Schemes to remove viral genome. (*B*) qRT-PCR of the SeV genome and hESC markers before and after temperature-shift treatment. iPSCs generated from HDF cells using TS7 vectors were treated with a temperature shift to 38 °C for 5 d. The SeV genome was not detected after this temperature-shift treatment, whereas expression of *NANOG* was not affected. (*C*) Schemes for generation of virus vector-free iPSCs from $CD34^+$ CB cells with SeV vectors. The ESC-like colonies 4, 15, and 17 that emerged were subcloned after heat treatment for 3 d at 38 °C. (*D* and *E*) The remaining SeV construct in SeV iPSC 4, SeV iPSC 15, and SeV iPSC 17 (*D*; passage 2, before heat treatment) and heat-treated subclone SeV iPSC 4A (from 4), SeV iPSC 15A (from 15), and SeV iPSC 17A (from 17) (*E*; passage 4) were determined by immunostaining with anti-HN antibody (*Left*) and by qRT-PCR against endogenous *NANOG* transcript and SeV RNA construct (*Right*). Retrovirally generated iPSCs from CB cells (Rev) and $CD34^+$ CB cells (CD34) were used as controls. The percentage of SeV-positive cells in the respective colony was determined using a two-value recognition function and is given below the qRT-PCR image.

during cell expansion (Fig. 2*C*). Almost all of the colonies picked up were virus-negative at late passages, and even if vectors were present, they could be easily removed using the temperature-shift protocol (Figs. 3*A* and 4). Indeed, the iPSCs generated using TS SeV vectors were free of any integrated viral factors, in contrast to retroviral-generated iPSCs, which express variable copy numbers of *OCT3/4*, *SOX2*, *KLF4*, and *c-MYC* (Fig. 3*D*). We also demonstrated that using TS SeV vectors, virus-negative iPSCs were efficiently generated from $CD34^+$ human CB cells (Fig. 4).

Although the use of synthetic modified mRNA to generate iPSCs has been reported, this is highly dependent on the gene delivery system, because it requires repetitive transfection for 16 d (13). Therefore, it might not be applicable to difficult-to-transfect cells, such as primary peripheral blood cells. The addition of decoy receptor to prevent IFN production by host cells is also needed. In contrast, SeV vectors require no transfection reagents or decoy receptors. We suggest that this is a considerable advantage to using nonintegrating SeV; the iPSCs thus generated have a homogeneous genetic background. Several studies on the generation of iPSCs from blood cells and CB cells with integration-free episomal vectors have been published recently (29–31). The efficiency of generating iPSCs is lower with episomal vectors than with SeV (>0.1% at an MOI of 2) and varies depending on the construction of the vectors and the nature of the transfection medium used. The major advantage of using nonintegrated SeV vectors is a potent and robust protein-expressing property that does not require optimization of the transfection medium. The volume of collected CB is 80–120 mL and may contain 2–4 $\times$ 10^5 $CD34^+$ cells on average. Our results show that only 1 $\times$ 10^4 $CD34^+$ cells, corresponding to ~5 mL of CB, are needed to obtain 10 independent iPSC clones with SeV. The rest of the CB can be sorted and used for the regular bone marrow transplantation therapy. In addition, there have been no reports of pathogenicity associated with SeV in primates, and the safety of the SeV vector is further enhanced by the F-deficiency that makes the vector nontransmissible (16).

In the present study, we have confirmed that the SeV vectors were not reactivated or detected in iPSCs at late passages or after temperature-shift treatment (Figs. 1*C* and 3). It has been suggested that TS mutations in *P* and *L* affect polymerase activity and promote degradation of the virus vector after treatment at nonpermissive temperatures (23). Based on our findings, we believe the TS SeV vector system that allows the elimination of remaining SeV construct from reprogrammed cells by temperature-shift treatment could accelerate future clinical application of iPSCs generated from cells obtained by less invasive or even noninvasive methods.

Materials and Methods

The induction of human iPSCs was done as reported previously (1, 17). Unless indicated otherwise, SeV vectors (*OCT3/4, SOX2, KLF4,* and *c-MYC*) were used at an MOI of 3 or 30 for 1 $\times$ 10^6 fibroblasts. For retroviral induction, fibroblasts were infected with mCAT containing simian immunodeficiency virus (SIV) vector at an MOI of 50, and then expanded by induction with retrovirus vectors containing reprogramming factors. Infected cells were transferred onto MMC-treated mouse embryonic fibroblast (MEF) feeder cells on day 6 after induction. Details of the experimental procedures are provided in *SI Materials and Methods*.

ACKNOWLEDGMENTS. We thank Satomi Nishikawa and K. Kobayashi for useful discussions; T. Aoi for RNA from hESCs; A. Iida for a critical reading of

the manuscript; T. Kitamura for pMX vector; RIKEN BioResource Center for CD34$^+$ CB cells; S. Seino, T. Kanaya, K. Washizawa, T. Fujikawa, E. Suzuki, and T. Yamamoto for technical assistance; H. Iwasaki for help with the histological studies; and T. Ofuji and M. Miyako for help with manuscript editing. This work was supported in part by the Japan Science and Technology Agency's Precursory Research for Embryonic Science and Technology and S-Innovation Programs, Regional Consortium Project Grant 19K5510 from the Ministry of Industry and Economy (2007–2009), Grant-in-Aid 2210853 from the Japan Society for the Promotion of Science Fellows, and Japan Science and Technology Agency "Tests for Safety Issue of Pluripotent Stem Cell" (2010-14).

1. Takahashi K, et al. (2007) Induction of pluripotent stem cells from adult human fibroblasts by defined factors. *Cell* 131:861–872.
2. Yu J, et al. (2007) Induced pluripotent stem cell lines derived from human somatic cells. *Science* 318:1917–1920.
3. Okita K, Nakagawa M, Hyenjong H, Ichisaka T, Yamanaka S (2008) Generation of mouse-induced pluripotent stem cells without viral vectors. *Science* 322:949–953.
4. Yu J, et al. (2009) Human induced pluripotent stem cells free of vector and transgene sequences. *Science* 324:797–801.
5. Soldner F, et al. (2009) Parkinson's disease patient–derived induced pluripotent stem cells free of viral reprogramming factors. *Cell* 136:964–977.
6. Sommer CA, et al. (2009) Induced pluripotent stem cell generation using a single lentiviral stem cell cassette. *Stem Cells* 27:543–549.
7. Stadtfeld M, Nagaya M, Utikal J, Weir G, Hochedlinger K (2008) Induced pluripotent stem cells generated without viral integration. *Science* 322:945–949.
8. Woltjen K, et al. (2009) piggyBac transposition reprograms fibroblasts to induced pluripotent stem cells. *Nature* 458:766–770.
9. Kaji K, et al. (2009) Virus-free induction of pluripotency and subsequent excision of reprogramming factors. *Nature* 458:771–775.
10. Jia F, et al. (2010) A nonviral minicircle vector for deriving human iPS cells. *Nat Methods* 7:197–199.
11. Zhou H, et al. (2009) Generation of induced pluripotent stem cells using recombinant proteins. *Cell Stem Cell* 4:381–384.
12. Kim D, et al. (2009) Generation of human induced pluripotent stem cells by direct delivery of reprogramming proteins. *Cell Stem Cell* 4:472–476.
13. Warren L, et al. (2010) Highly efficient reprogramming to pluripotency and directed differentiation of human cells with synthetic modified mRNA. *Cell Stem Cell* 7: 618–630.
14. Lamb RA, Kolakofsky D (1996) Paramyxoviridae: The viruses and their replication. Fields Virology, eds Fields BN, Knipe DM, Howley PM (Lippincott-Raven, Philadelphia), 3rd Ed, pp 1177–1204.
15. Li HO, et al. (2000) A cytoplasmic RNA vector derived from nontransmissible Sendai virus with efficient gene transfer and expression. *J Virol* 74:6564–6569.
16. Nagai Y, Takakura A, Irie T, Yonemitsu M, Gotoh B (2011) Evolution of Sendai virus: The journey from mouse pathogen to a state-of-the-art tool in virus research and biotechnology. The Paramyxoviruses, ed Samal SK (Horizon Scientific Press, Norwich, UK).
17. Fusaki N, Ban H, Nishiyama A, Saeki K, Hasegawa M (2009) Efficient induction of transgene-free human pluripotent stem cells using a vector based on Sendai virus, an RNA virus that does not integrate into the host genome. *Proc Jpn Acad, Ser B, Phys Biol Sci* 85:348–362.
18. Seki T, et al. (2010) Generation of induced pluripotent stem cells from human terminally differentiated circulating T cells. *Cell Stem Cell* 7:11–14.
19. Jin CH, et al. (2003) Recombinant Sendai virus provides a highly efficient gene transfer into human cord blood–derived hematopoietic stem cells. *Gene Ther* 10:272–277.
20. Giorgetti A, et al. (2009) Generation of induced pluripotent stem cells from human cord blood using OCT4 and SOX2. *Cell Stem Cell* 5:353–357.
21. Takenaka C, Nishishita N, Takada N, Jakt LM, Kawamata S (2010) Effective generation of iPS cells from CD34$^+$ cord blood cells by inhibition of p53. *Exp Hematol* 38:154–162.
22. Bowman MC, Smallwood S, Moyer SA (1999) Dissection of individual functions of the Sendai virus phosphoprotein in transcription. *J Virol* 73:6474–6483.
23. Feller JA, Smallwood S, Skiadopoulos MH, Murphy BR, Moyer SA (2000) Comparison of identical temperature-sensitive mutations in the L polymerase proteins of Sendai and parainfluenza3 viruses. *Virology* 276:190–201.
24. Inoue M, et al. (2003) Nontransmissible virus-like particle formation by F-deficient Sendai virus is temperature-sensitive and reduced by mutations in M and HN proteins. *J Virol* 77:3238–3246.
25. Guo XM, et al. (2006) Creation of engineered cardiac tissue in vitro from mouse embryonic stem cells. *Circulation* 113:2229–2237.
26. D'Amour KA, et al. (2005) Efficient differentiation of human embryonic stem cells to definitive endoderm. *Nat Biotechnol* 23:1534–1541.
27. Kawasaki H, et al. (2000) Induction of midbrain dopaminergic neurons from ES cells by stromal cell–derived inducing activity. *Neuron* 28:31–40.
28. Majeti R, Park CY, Weissman IL (2007) Identification of a hierarchy of multipotent hematopoietic progenitors in human cord blood. *Cell Stem Cell* 1:635–645.
29. Chou BK, et al. (2011) Efficient human iPS cell derivation by a non-integrating plasmid from blood cells with unique epigenetic and gene expression signatures. *Cell Res* 21: 518–529.
30. Hu K, et al. (2011) Efficient generation of transgene-free induced pluripotent stem cells from normal and neoplastic bone marrow and cord blood mononuclear cells. *Blood* 117:e109–e119.
31. Yu J, Chau KF, Vodyanik MA, Jiang J, Jiang Y (2011) Efficient feeder-free episomal reprogramming with small molecules. *PLoS ONE* 6:e17557.

Biomaterials 32 (2011) 3555–3563

Contents lists available at ScienceDirect

Biomaterials

journal homepage: www.elsevier.com/locate/biomaterials

The use of leukemia inhibitory factor immobilized on virus-derived polyhedra to support the proliferation of mouse embryonic and induced pluripotent stem cells

Naoki Nishishita [a,b,1], Hiroshi Ijiri [c,1], Chiemi Takenaka [a,b], Kenichiro Kobayashi [b], Kohei Goto [c], Eiji Kotani [c], Tohru Itoh [d], Hajime Mori [c,e,**], Shin Kawamata [a,b,*]

[a] Foundation for Biomedical Research and Innovation TRI308, 1-5-4 Minatojima-Minamimachi, Chuo-ku, Kobe 650-0043, Japan
[b] Riken Center for Developmental Biology, 2-2-3 Minatojima-Minamimachi, Chuo-ku, Kobe 650-0047, Japan
[c] Insect Biomedical Research Center, Kyoto Institute of Technology, Matsugasaki, Sakyo-ku, Kyoto 606-8585, Japan
[d] TC Reagent Group, Consumer Products Division, Production General Division, AGC Techno Glass Co., Ltd., 1-50-1 Gyoda, Funabashi 273-0044, Japan
[e] Protein Crystal Corporation, 1-12-8 Senba Higashi, Minoh 541-0053, Japan

ARTICLE INFO

Article history:
Received 8 December 2010
Accepted 29 December 2010
Available online 18 February 2011

Keywords:
LIF
Polyhedra
Slow release
ES cells
iPS cells

ABSTRACT

Human leukemia inhibitory factor (LIF) was immobilized into insect virus-derived microcrystals (polyhedra) to generate LIF polyhedra (LIF-PH) that can slowly release LIF into embryonic stem (ES) cell culture media and thus maintain ES cells in an undifferentiated state. Assays of the biological activities of LIF-PH indicated that a single addition of LIF-PH to the ES cell culture medium can support the proliferation of mouse ES and induced pluripotent stem (iPS) cells continuously for 14 days, and suggest that LIF-PH can be successfully used in the place of a periodic addition of recombinant LIF to the media every 2–3 days. The release of LIF protein from LIF-PH was determined by enzyme-linked immunosorbent assay (ELISA). Maintenance of undifferentiated state of mouse ES and iPS cells cultured with LIF-PH was determined by the detection of pluripotency-related biomarkers Oct3/4 and stage-specific embryonic antigen-1 (SSEA-1) through immunostaining and measurement of alkaline phosphatase activity. In this paper, we propose a closed culture system for mass production of ES and iPS cells that utilize a slow-releasing agent of LIF.

1. Introduction

Leukemia inhibitory factor (LIF) initially was identified as a cytokine capable of inducing the differentiation of M1 myeloid leukemia cells, and later was shown to have a strong differentiation-inhibiting activity on embryonic stem (ES) cells [1,2]. At present, mouse ES cells are cultured in an undifferentiated state on gelatin-coated polystyrene plates in the presence of LIF [3,4]. LIF belongs to the family of interleukin-6 (IL-6)-type cytokines. This family of cytokines stimulates target cells through the gp130 receptor, which is expressed in all cells of the body, while the specific cytokine receptor subunits are expressed in a cell-specific manner and induce a specific cellular response when triggered by a particular member of the cytokine family. LIF induces heterodimerization of the gp130 and LIF receptor (LIFR) upon binding to receptor subunits, and this dimerization results in the activation of associated Jak tyrosine kinases and initiation of intracellular signaling cascades [5]. Jak-mediated phosphorylation of specific tyrosine residues in the gp130 cytoplasmic domain creates docking sites for Src homology 2-containing signal transducer and activator of transcription (STAT) proteins, which are then phosphorylated and translocate to the nucleus as dimers to induce expression of specific sets of genes [6,7]. The STAT protein family has seven members, of which STAT3 is the major mediator of gp130 signals [8]. STAT3 is thought to be involved in the induction of a set of genes related to maintenance of pluripotency and self-renewal in ES cells [9,10]. Previous reports indicate that mouse LIF binding activity is specific to mouse LIFR, while human LIF can bind LIFR from either human or mouse. In addition, the binding activity of human LIF to mouse LIFR is higher than that of mouse LIF [11,12].

The disruption or removal of LIF signaling (e.g. by cytokine starvation) will trigger a signal within stem cells to differentiate [13]. Presumably, continuous activation of LIF-mediated signaling by a slow, steady release of LIF in cell culture, rather than spikes in activation and rapid withdrawal of LIF-mediated signaling observed

* Corresponding author. Foundation for Biomedical Research and Innovation TRI308, 1-5-4 Minatojima-Minamimachi, Chuo-ku, Kobe 650-0043, Japan. Tel.: +81 78 306 0681; fax: +81 78 306 0391.
** Corresponding author. Insect Biomedical Research Center, Kyoto Institute of Technology, Matsugasaki, Sakyo-ku, Kyoto 606-8585, Japan. Tel./fax: +81 75 724 7776.
E-mail addresses: hmori@kit.ac.jp (H. Mori), kawamata@fbri.org (S. Kawamata).
[1] These authors contributed equally to this work.

0142-9612/$ – see front matter © 2011 Elsevier Ltd. All rights reserved.
doi:10.1016/j.biomaterials.2010.12.063

during periodic addition of recombinant LIF would be beneficial for maintaining stem cell pluripotency during self-renewal. For this purpose, we have developed a new slow-releasing agent comprised of a viral protein crystalline matrix containing immobilized human LIF molecules.

Cypovirus (CPV) infections of insect larvae are characterized by the production of massive amounts of a major virus-encoded protein (polyhedrin). The polyhedrin protein molecules crystallize in the cell cytoplasm to form cubic inclusion bodies (polyhedra) that incorporate numerous virus particles. CPVs belong to a genus within the *Reoviridae* family [14]. Polyhedra function to facilitate the survival of the incorporated virus in hostile environments, stabilizing the virions and allowing long-term viability. These polyhedra are also highly resistant to both nonionic and ionic detergents and are soluble at neutral pH [15]. Previously, we have produced recombinant polyhedra derived from *Bombyx mori* cypovirus (BmCPV) without incorporation of virus particles. We developed two targeting strategies for the incorporation of foreign proteins into polyhedra. Diverse foreign proteins can be immobilized into polyhedra by fusing a polyhedron-targeting tag sequence at the C- or N-terminus of the foreign protein [16].

As described in this report, we have generated two types of polyhedra by immobilizing human LIF fused with a polyhedron-targeting tag sequence at either the C- or N-terminus. The biological effects of these polyhedra on cultured stem cells were determined and compared to those effects seen when using recombinant human LIF (rhLIF) in analogous experiments.

2. Materials and methods

2.1. Generation of LIF polyhedra

Recombinant LIF baculovirus transfer vectors were generated using GATEWAY® cloning technology (Invitrogen). The LIF gene fused to DNA encoding either the VP3 or the H1 immobilization signal was amplified by polymerase chain reaction (PCR) using primer sets containing *att*B1 and *att*B2 sequences. The forward primer 5′-GGGGACAAGTTTGTACAAAAAAGCAGGCTTAATGAAGGTCTTGGCGGCAGGAG-3′ and reverse primer 5′-GGGGACCACTTTGTACAAGAAAGCTGGGTAGAAGGCCTGGGCCAACACGGCG-3′ were used to amplify the LIF gene coupled to DNA encoding the VP3 immobilization signal, and the forward primer 5′-GGGGACAAGTTTGTACAAAAAAGCAGGCTTAAAGGTCTTGGCGGCAGGAGTTG-3′ and reverse primer 5′-GGGGACCACTTTGTACAAGAAAGCTGGGTGCTAGAAGGCCTGGGCCAACACGGCG-3′ were used to amplify the LIF gene fused to DNA encoding the H1 immobilization signal. The resulting *att*B-flanked PCR products were cloned into a donor vector (pDONR221) by BP reactions of GATEWAY® system. To produce transfer vectors encoding H1 or VP3 immobilization signals, the open reading frame cloned between the *att*L1 and *att*L2 sites in the entry vectors was transferred to destination vectors (pDEST-C-VP3 or pDEST-N-H1) via LR Clonase™ reactions. The resulting transfer vectors were co-transfected into *Spodoptera frugiperda* IPLB-Sf21-AE (Sf21) cells with linearized Baculogold Baculovirus DNA (BD Pharmingen), and replication-competent baculovirus was rescued by recombination between transfer vector and the linearized viral DNA and ultimately harvested from the supernatant. Immobilization of LIF using VP3 or H1 signals was accomplished by dual infection of the recombinant baculoviruses that express the LIF fusion proteins and a recombinant baculovirus AcCP-H expressing BmCPV polyhedrin. The resulting polyhedra were recovered and purified from Sf21 cells, and detected by western blotting as previous reported in Reference [16]. Polyhedra were stored in distilled water containing penicillin (100 U/mL) and streptomycin (100 μg/mL).

2.2. Cell culture

The mouse ES cell line, EB5, was derived from *E14tg2a* (ATCC) by inserting the *Aspergillus terreus* blasticidin S deaminase gene and was provided by Dr. Niwa (Riken CDB, Kobe), and maintained as previously described in References [3,4]. In brief, EB5 cells were maintained on 6-well plates (Asahi Glass) coated with 0.1% type A gelatin (Sigma–Aldrich) in undifferentiation medium ["glow minimum essential medium" (GMEM; Invitrogen) supplemented with 1% fetal bovine serum (FBS; CELLect, MP Bioscience), 10% KnockOut Serum Replacement (KSR; Invitrogen), 0.1 mM nonessential amino acids (NEAA; Invitrogen), 1 mM sodium pyruvate (Invitrogen), 0.1 mM 2-mercaptoethanol, blasticidin (500 ng/mL; Invitrogen), and 2000 U/mL (10 ng/mL) rhLIF (Chemicon International LIF1005)]. Cultivation of undifferentiated EB5 cells harboring a blasticidin resistant gene that is fused to the *Oct-4* promoter region was achieved through blasticidin selection. EB5 passaging was accomplished by washing cells once with phosphate-buffered saline (PBS) and then incubating with 0.05% trypsin-ethylenediaminetetraacetic acid (EDTA) at 37 °C for 5 min. Cell clumps were dissociated completely by pipetting in undifferentiation medium. Ten thousand cells were seeded in a 6-well plate and cultured in 2 mL of undifferentiation medium for 3 days before the next passage.

To generate mouse iPS cells, neural stem cells (NSCs) isolated from Oct-4/green fluorescent protein (GFP) transgenic mice [17] were used as cell source for reprogramming. One hundred thousand NSCs were transduced with retroviruses bearing *c-Myc*, *Klf4*, *Oct3/4* and *Sox2* genes as described in Reference [18]. Twenty-four hours post-transduction, cells were transferred to ES medium and maintained in feeder-free gelatin-coated plates. Oct-4-GFP positive cells emerged within 1 week and iPS cells (IWF-1; named after iPSc Without Feeder cell) were established in 3 weeks. Silencing of the exogenous factor and reactivation of the series of endogenous pluripotency markers were confirmed by reverse transcription (RT)-PCR. Generation of chimeric mice was confirmed following blastocyst injection.

2.3. Cell proliferation assay

For both short-term (7 days) and for long-term culture (14 days) culture, 2×10^5 cubes or 5×10^5 cubes of polyhedra containing either H1-tagged LIF (H1/LIF polyhedra) or VP3-tagged LIF (LIF/VP3 polyhedra) were mixed in 0.1% gelatin solution, coated on a polystyrene plate, and air-dried at room temperature. Cells were harvested and counted at indicated days.

2.4. Immunostaining of ES cell undifferentiation markers

Mouse ES or iPS cells were cultured with either 2×10^5 cubes of H1/LIF polyhedra, LIF/VP3 polyhedra, empty polyhedra (CP-H polyhedra), 10 ng/mL of rhLIF, or without rhLIF in the absence of blasticidin for 3 days. Cells were then fixed in 4% paraformaldehyde in permeabilization solution (0.2% Triton X-100 in PBS) for 20 min at 4 °C, rinsed with PBS, and then blocked in a blocking buffer (PBS containing 0.1% bovine serum albumin (BSA)) for 15 min at room temperature. The ES cells were incubated with a 1:100 dilution of primary antibody against Oct-4 (Santa Cruz Biotechnology, catalog #SC-5279) or against stage-specific embryonic antigen-1 (SSEA-1; Santa Cruz Biotechnology, catalog #SC-21702), and mouse iPS cells were incubated with primary antibody against SSEA-1 at 4 °C overnight followed by incubation with Alexa fluorophores (Invitrogen) for 1 h at 37 °C. Alkaline phosphatase (ALP) activity of cultured cells was detected with a Vector Blue® Alkaline Phosphatase Subtraction Kit (Vector Laboratories) according to the manufacturer's instructions. Cells were observed by either fluorescence microscopy or by phase-contrast microscopy using an Olympus CKX-31 inverted microscope.

2.5. Enzyme-linked immunosorbent assay (ELISA)

Concentration of LIF in culture media was determined by ELISA. Two hundred thousand cubes of CP-H polyhedra or either LIF/VP3 or H1/LIF polyhedra were added in undifferentiation medium to 1×10^5 EB5 cells. The release of LIF from polyhedra in fresh undifferentiation medium was measured at days 0 (1 h after adding polyhedra to the cell culture), 1, 2, 3, 4 or 5, and was determined using a Human LIF Quantikine ELISA kit (R&D Systems) in accordance with the manufacturer's protocol. The release of LIF from polyhedra in a conditioned medium harvested from culture medium used to keep EB5 in confluence for 24 h was also determined with this kit. The amount of soluble LIF was measured by absorbance at 450 nm with a microplate reader (Model 680, Bio-Rad).

Activation of STAT3 was also determined by ELISA. Ten thousand EB5 cells were cultured without rhLIF in the presence of blasticidin for 3 days to generate a LIF starvation culture, and then either 2×10^6 cubes of H1/LIF polyhedra or 10 ng/mL rhLIF was added to the cell culture. The cells were harvested at designated time points, mixed with ice-cold cell lysis buffer (Cell Lysis Buffer (10×); Cell Signaling) with 1 mM phenylmethylsulfonyl fluoride (PMSF; Sigma) and incubated at 4 °C for 5 min after assessing the cell number. The cell lysate was centrifuged at 14000×g for 10 min at 4 °C, and the supernatant was then collected. Soluble phospho-STAT3 (Y705) levels in the supernatant were measured by ELISA using a PathScan® plate in accordance with the manufacturer's protocol. Horse radish peroxidase (HRP)-conjugated antibody was used for the detection of phospho-STAT3, and absorbance at 450 nm was measured with a microplate reader (Model 680, Bio-Rad).

2.6. Western blotting

Analysis by sodium dodecyl sulfate-polyacrylamide gel electrophoresis (SDS-PAGE) and western blot detection was performed by suspending 4×10^5 cubes of each type of polyhedra in 30 μL of SDS-PAGE sample buffer (50 mM Tris–HCl (pH 6.8), 100 mM dithiothreitol, 2% SDS, 0.1% bromophenol blue, and 10% glycerol), followed by boiling for 5 min, cooling on ice, and separating the polyhedra lysates by SDS-PAGE at 25 mA. Duplicate lanes for each polyhedra sample were prepared, and following electrophoresis one-half of the gel was transferred onto a nitrocellulose membrane at 54 mA for 90 min for western blotting while the other half was stained with coomassie blue. The blotted membrane was incubated with an anti-human LIF monoclonal primary antibody (R&D systems) diluted 1:250 in 3% skim milk/Tris-buffered

saline with Tween-20 (TBS-T) for 2 h at 25 °C, followed by a second incubation at 25 °C for 2 h with an HRP-conjugated anti-mouse secondary antibody (Bio-Rad) diluted 1:3000 in 3% skim milk/TBS-T. After several washes, the membrane was developed with an immunostaining kit (HRP-1000; Konica) according to the manufacturer's instructions.

3. Results

3.1. Immobilization of human LIF into BmCPV polyhedra

The viral protein VP3 mediates incorporation of BmCPV into polyhedra, and a stretch of 52 amino acids within this protein is sufficient to direct immobilization of foreign proteins into polyhedra. This 52-aa sequence was fused to the C-terminus of LIF to direct LIF uptake into polyhedra, and is termed VP3-tag. Similarly, a stretch of 30 amino acids from the N-terminal alpha helix of the BmCPV polyhedrin protein can be used to direct immobilization of foreign proteins into the cubic polyhedra structure [15,16,19], and this 30-aa sequence (termed H1-tag) was fused to the N-terminus of LIF to direct LIF immobilization into polyhedra. Human LIF protein bearing either a VP3-tag or a H1-tag was immobilized into polyhedra to generate two types of LIF polyhedra that can slowly release LIF into the culture medium, namely H1/LIF polyhedra and LIF/VP3 polyhedra. The amount of immobilized LIF, the LIF release rate from polyhedra, and the biological activities of the released protein were examined in biological assays, with the two tagging methods yielding differing outcomes.

The schema for generation of the two types of LIF polyhedra and photos of LIF polyhedra are shown in Fig. 1A. Immobilization of LIF protein into polyhedra was confirmed by the detection of LIF protein by western blotting (Fig. 1B). LIF protein can be immobilized into polyhedra by either the H1-tag or the VP3-tag. However, the intensity of LIF bands in the western blot indicates that LIF protein was more efficiently immobilized into polyhedra when the H1-tag was used.

3.2. Release of LIF in cell culture media

Release of LIF from H1/LIF and LIF/VP3 polyhedra in culture medium was determined by ELISA. Ten thousand EB5 cells were cultured with 2×10^5 cubes of H1/LIF polyhedra, and release of LIF was observed 1 h after the culture was initiated (day 0). However, the same dose of LIF/VP3 polyhedra did not release detectable levels of LIF, with measurements showing only background-level signals, as low as empty polyhedra (CP-H polyhedra) derived from an infection of Sf21 cells with AcCP-H alone (Fig. 2). The release of LIF from H1/LIF polyhedra peaked 2 days after the culture was initiated, and lasted as long as 5 days so far measured. On the other hand, rhLIF levels begin to diminish at day 3 and are drastically reduced at day 4 days, with levels almost 1/10 of the initial dose. The rhLIF levels were barely detectable at day 6. Interestingly, the amount of rhLIF added to the cell culture is drastically reduced within 1 h. A likely explanation for this drop is that some portion of rhLIF binds to LIF receptor, while the majority of rhLIF molecules stick to the wall of culture dishes or are degraded soon after addition to the cell culture media. The release of LIF was observed within 1 h when H1/LIF polyhedra were soaked in fresh cell culture media (without cells), but not in PBS (Fig. 2). Also interestingly, the amount of LIF released was suppressed when H1/LIF polyhedra were incubated with conditioned media alone (without cells) or added to overgrown EB5 cell culture that had been cultured with mouse recombinant LIF. The ELISA kit used in these studies detects rhLIF but not mouse recombinant LIF (data not shown). These data suggest that the culture media may contain substance(s) that promotes the degradation of polyhedra, while the conditioned media may have factor(s) that antagonize or neutralize such putative digestive activities of substance(s) found in fresh culture media.

3.3. Maintenance of pluripotent stem cells with H1/LIF polyhedra

Colonies of pluripotent mouse ES or iPS cells having a dome-like morphology require a continuous supply of LIF to proliferate in the undifferentiated state, while the colonies start to differentiate and become flat or take on an epithelium-like appearance in the absence of LIF. EB5 cells cultured with rhLIF or on H1/LIF or LIF/VP3 polyhedra-coated 6-well plates are shown in Fig. 3. Notably, the cell culture with 2×10^5 cubes of H1/LIF polyhedra, as well as that with 10 ng/mL rhLIF, maintained dome-shape colonies that were positively-stained with ALP, but such findings from the culture with the same dose of LIF/VP3 polyhedra were not observed (Fig. 3). In accord with the LIF release data shown in Fig. 2, these results suggest that the level of LIF release from LIF/VP3 polyhedra was not sufficient to maintain the undifferentiated state of mouse ES or iPS cells. The maintenance of the undifferentiated stage of pluripotent stem cells was further evaluated by the detection of pluripotency-related biomarkers such as Oct3/4 or SSEA-1. Mouse ES cell colonies maintained a dome-like appearance and retained the expression of Oct3/4 and SSEA-1 molecules when the cells were cultured with 2×10^5 cubes of H1/LIF polyhedra or 10 ng/mL of rhLIF, but not with LIF/VP3 polyhedra or with CP-H polyhedra (Fig. 4A and B). An epithelium-like colony emerged and loss of SSEA-1 or Oct3/4 expression was observed when the cells were cultured in the absence of rhLIF (data not shown), as was observed in cell cultures with CP-H or LIF/VP3 polyhedra.

Like the mouse ES cell colonies, mouse Oct-4-GFP knock-in iPS cell colonies (iWF-1) cultured with rhLIF and H1/LIF maintained a dome-shape morphology, SSEA-1 expression at a molecular level, and Oct3/4 at a transcriptional level, but such cultures in the presence of LIF/VP3 or CP-H polyhedra did not (Fig. 4C and D), analogous to the results shown in Fig. 3. Morphology of the iPS cell colonies cultured with LIF/VP3 polyhedra was distinct from that with H1/LIF polyhedra. Dish-like colonies emerged when cultured with LIF/VP3, but the rim of these colonies were detached from the gelatin-coated dish and formed embryoid body-like cell clumps. These cell clusters did not express SSEA-1 at the center of the colony. Interestingly, EB5 cells spontaneously start to differentiate as an adhesive cell, while iWF-1 cells lose adhesive properties and start to differentiate following LIF depletion. It is presumed that difference in epigenetic status may account for a distinct cellular behavior in differentiation upon LIF depletion in these two cell lines. The exact mechanism shall be elucidated in future study.

3.4. Addition of H1/LIF polyhedra sustains ES cell growth in a dose-dependent manner

The effect of LIF polyhedra on mouse ES iPS cell proliferation during short-term (7-day) culture was determined by assessing cell number at days 3 and 5. Of particular note, the proliferation potential afforded by 2×10^5 cubes of H1/LIF polyhedra is equivalent to that of 10 ng/mL rhLIF and far superior to that of LIF/VP3 (Fig. 5A and C). In addition, ES cells proliferated in a dose-dependent manner within the range of 7.5×10^3 to 2×10^5 cubes of H1/LIF polyhedra (Fig. 5B).

The slow release effect of H1/LIF polyhedra was determined by assessing cell number during ES cell culture over 2 weeks. ES cells were cultured either with 2×10^5 cubes or 5×10^5 cubes of H1/LIF polyhedra or 10 ng/mL rhLIF, and cell numbers were determined at days 3, 5, 7, and 14. The rhLIF was added to the culture media at days 0, 3, 5, 7, 10 and 12 to sustain cell proliferation, while H1/LIF polyhedra were added just once, at the start of the culture. H1/LIF

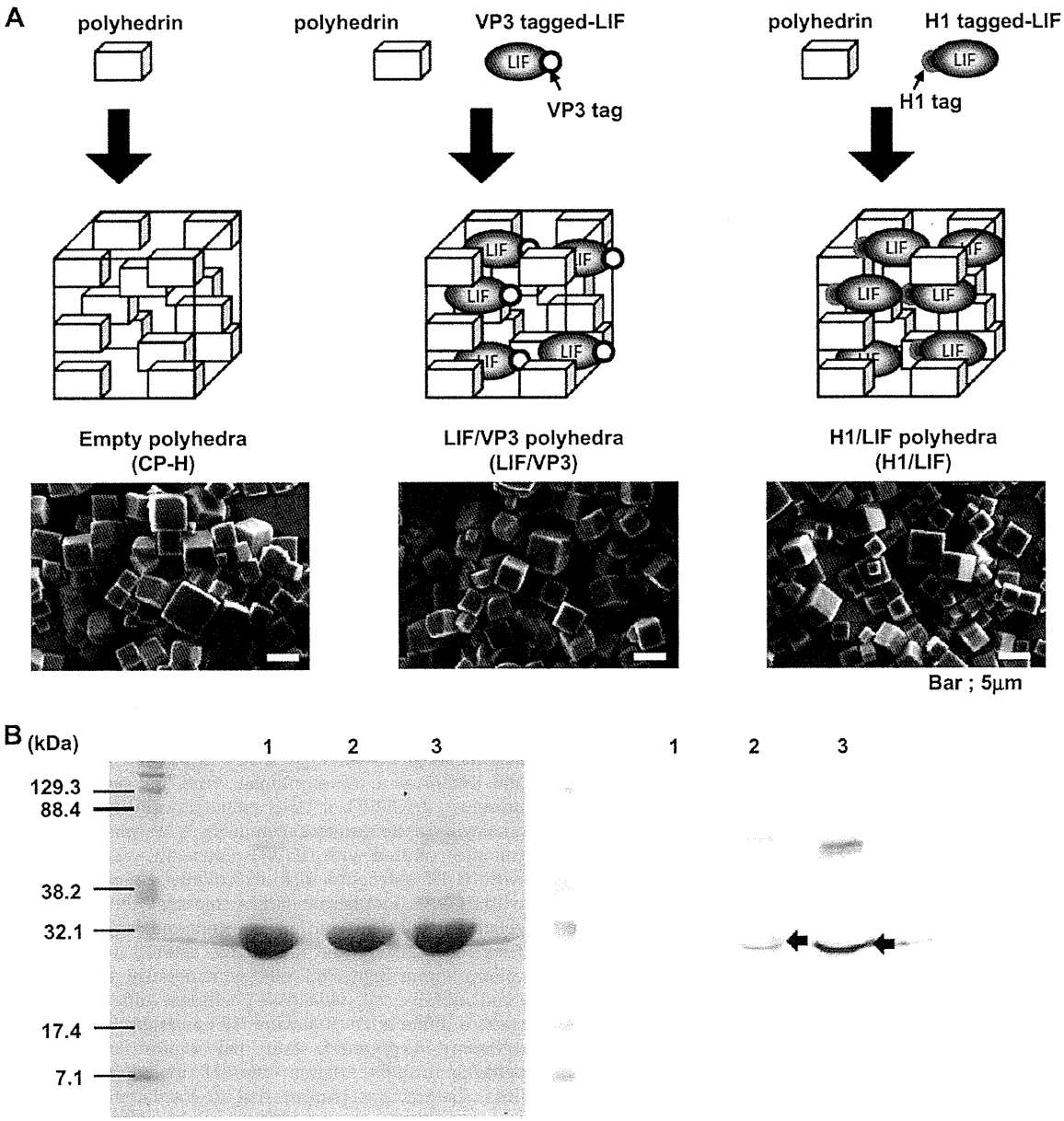

Fig. 1. (A) Schema for the generation of LIF slow-releasing agents (LIF-containing polyhedra), and corresponding photos of polyhedra crystals. Either H1-tagged LIF or VP3-tagged LIF was immobilized into polyhedra to generate two types of slow-releasing agents, namely H1/LIF polyhedra (H1/LIF) or LIF/VP3 polyhedra (LIF/VP3). Empty polyhedra (CP-H) consisting solely of BmCPV polyhedrin protein were used as a control. (B) Detection of LIF immobilized into polyhedra by SDS-PAGE and western blotting. LIF immobilized into polyhedra was analyzed by electrophoresis on 12.5% polyacrylamide gels (left panel) and detected by western blotting (right panel) with an anti-LIF monoclonal antibody. Lanes 1, 2, and 3 correspond to CP-H, LIF/VP3, and H1/LIF samples, respectively. Arrows show the bands corresponding to human LIF molecule.

polyhedra showed a slow-releasing effect, as 5×10^5 cubes of H1/LIF polyhedra sustained ES cell proliferation at a comparable level to that seen with the cell culture where 10 ng/mL rhLIF is added every 2–3 days (Fig. 5D).

3.5. Signaling delivered by H1/LIF polyhedra is persistent

Propagation of LIF-stimulated intracellular signaling is mediated by STAT3 activation [20], which can be determined by the detection of phosphorylated STAT3. Indeed, addition of rhLIF or H1/LIF polyhedra to a rhLIF-starved EB5 cell culture induced a spike in STAT3 phosphorylation at 3 and 6 h (Fig. 6). The STAT3 phosphorylation induced by rhLIF rapidly falls to basal levels by day 3 at the single cell level, and additional 10 ng/mL rhLIF is needed to resume increased STAT3 phosphorylation levels. STAT3 phosphorylation was also assayed 6 h after the addition of rhLIF on days 3 and 5. A similar induction of STAT3 phosphorylation was observed 6 h after adding rhLIF on days 3 and 5 of the culture followed by reduction of STAT3 phosphorylation at days 5 and 7. However, the magnitude of the phospho-STAT3 induction is attenuated over the course of the culture at the single cell level due to an increased total cell number (Fig. 6). In contrast, when 2×10^5 cubes of H1/LIF polyhedra were

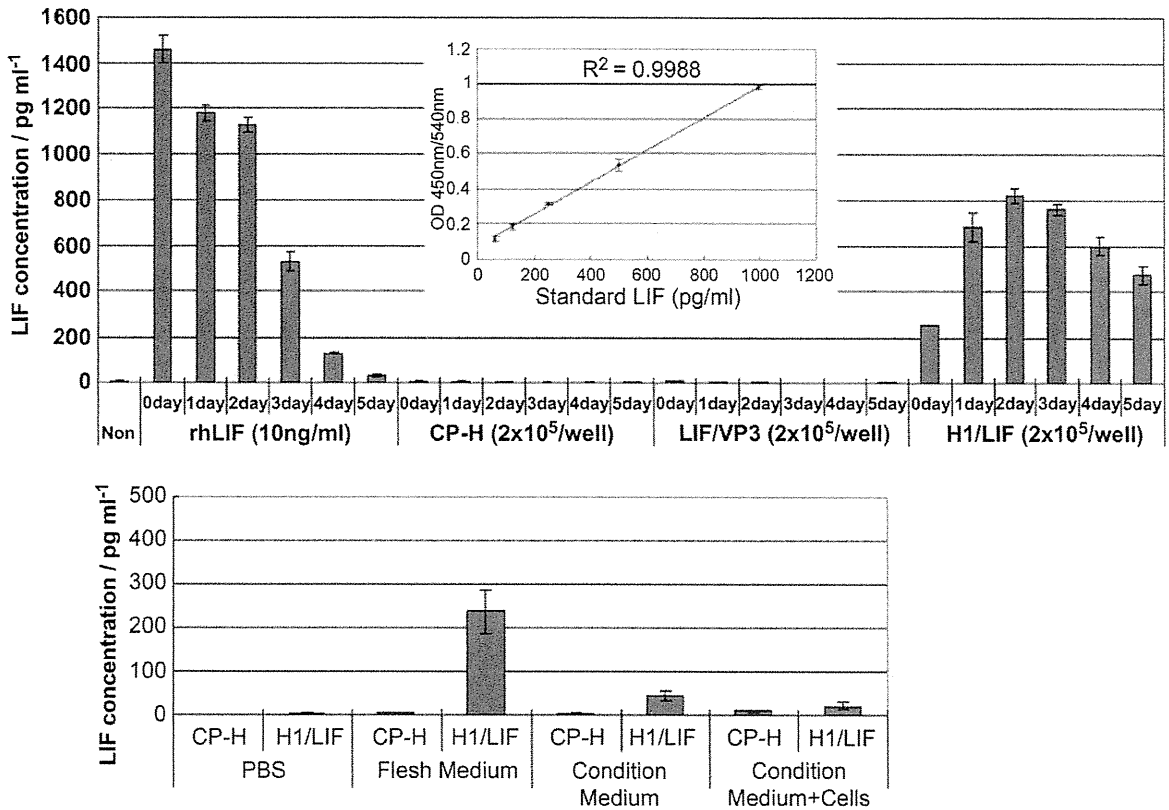

Fig. 2. Concentration of human LIF in ES cell culture media from designated culture conditions. ES cells were cultured either with 10 ng/mL rhLIF, or with 2×10^5 each of cubes of empty CP-H polyhedral (CP-H), LIF/VP3 polyhedra (LIF/VP3), or H1/LIF polyhedra (H1/LIF) (Upper panel). The amount of LIF in culture media from an individual sample was determined by ELISA and the measured value is shown as a bar, with an error bar indicating standard deviation (*X*-axis, different treatments and times; *Y*-axis, amount in pg/ml). Samples taken 1 h after the culture was initiated were designated as being collected at day 0. In addition, the amount of human LIF released from 2×10^5 cubes of CP-H or H1/LIF polyhedra that were suspended for 1 h in PBS, fresh media for EB5 (Fresh Medium), conditioned media from 3-day-old EB5 culture (Condition Medium), or 3-day-old EB5 cell culture (Condition Medium + Cells) was also determined (Lower panel). The inset shows the calibration curve and the best-fit lines used for converting optical density (OD) to concentration values.

added to EB5 cells at the start of the culture, the sharp activation of STAT3 decreases slowly over time, as determined by measurements made at day 3 + 6 h, day 5 + 6 h, and day 7 + 6 h. The concentration of LIF in culture media under various culture conditions shown in Fig. 2 also supported these results.

4. Discussion

Our study demonstrates that H1/LIF polyhedra, which immobilized human LIF into polyhedra via the H1-tag, possess long-acting biological activities in ES cell culture, with effects comparable to

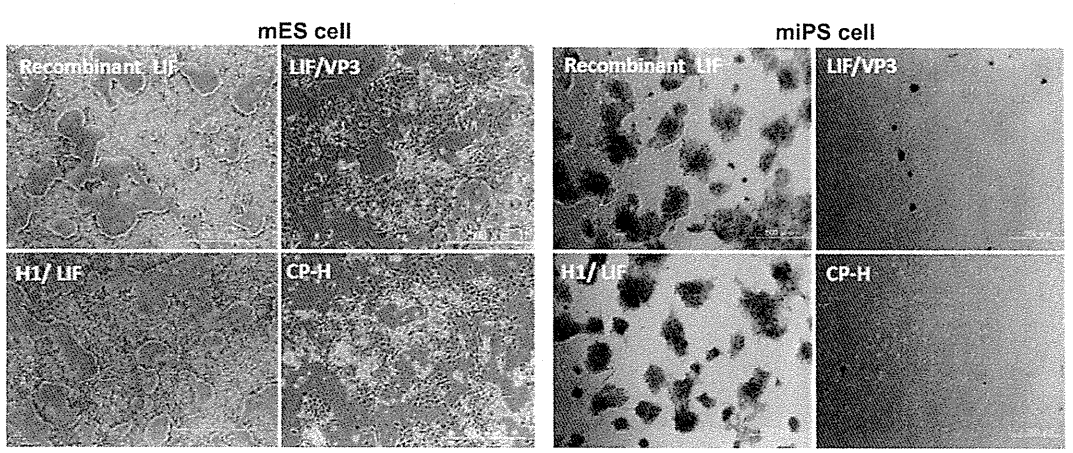

Fig. 3. Biological effect of H1/LF and LIF/VP3 on the maintenance of ES cells. Mouse ES cells (EB5 cells; left panels) or mouse iPS cells (iWF-1 cells; right panels) were cultured with 10 ng/mL rhLIF (upper left) or with 2×10^5 cubes of LIF/VP3 (upper right), H1/LIF (lower left) or CP-H (lower right) polyhedra for 5 days, followed by ALP staining.

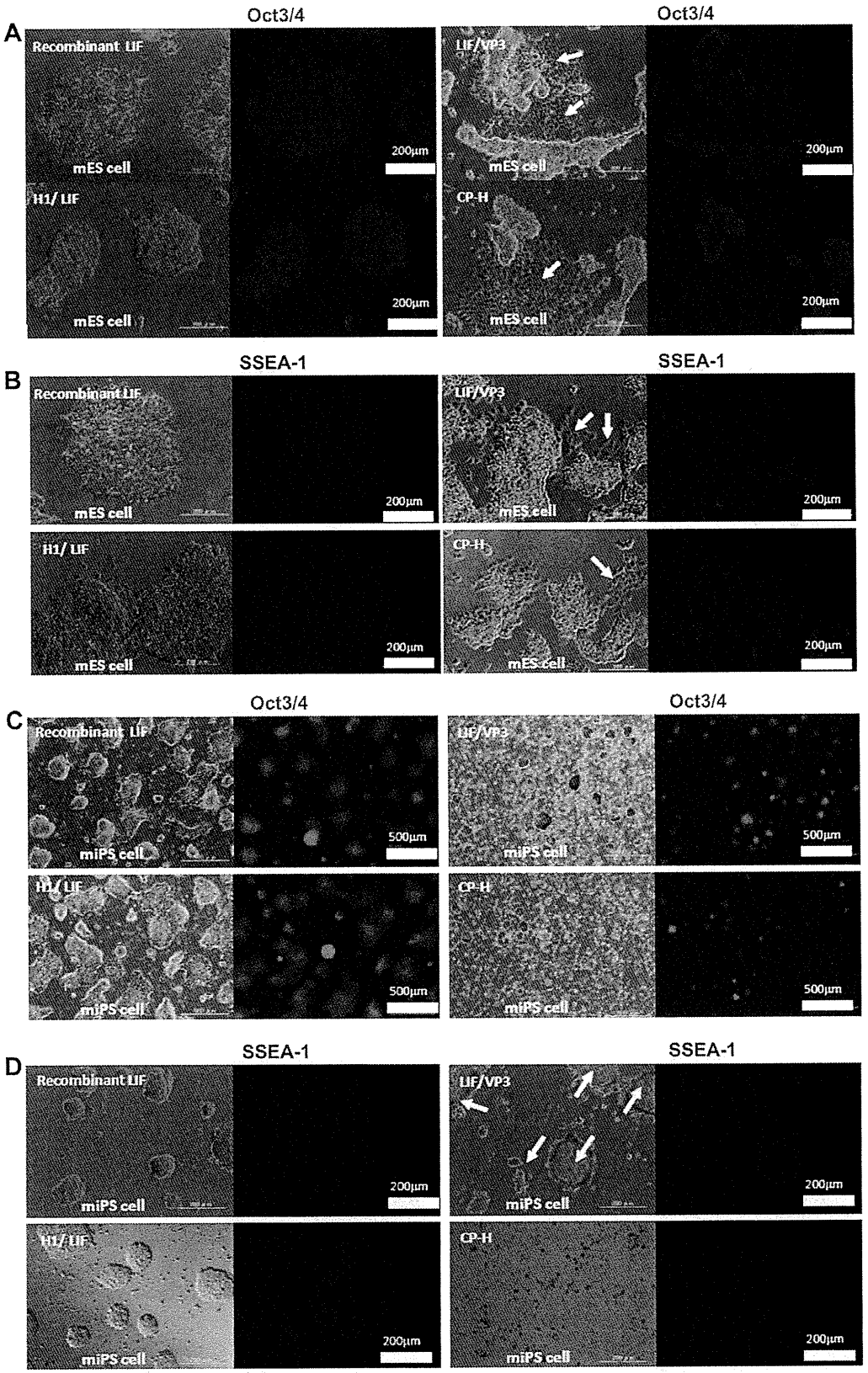

Fig. 4. Expression of pluripotency-related markers in ES cells cultured with polyhedra. Expression of Oct3/4 (A), SSEA-1 (B) in cultured EB5 cells, or Oct3/4 (C), SSEA-1 (D) in cultured mouse iPS cells (iWF-1 cells) with 10 ng/mL rhLIF (upper left) or 2×10^5 cubes of LIF/VP3 (upper right), H1/LIF (lower left) or CP-H (lower right) polyhedra are shown. Cells were cultured with respective agents for 5 days and fixed for immunostaining. A phase-contrast image (left) and the corresponding immunostaining image (right) under a fluorescent microscope are shown.